University of Thessaly

School of Engineering

Department of Mechanical Engineering

Master Thesis

Design of a Vibration Measurement System for the Metsovo Bridge

by

Costas Argyris

Diploma in Mechanical Engineering, University of Thessaly, 2011

A Thesis
Submitted in Partial Fulfillment of the
Requirements for the Degree of
Master of Science
(in Mechanical Engineering)

2013

Πανεπιστήμιο Θεσσαλίας

Πολυτεχνική Σχολή

Τμήμα Μηχανολόγων Μηχανικών

Μεταπτυχιακή Εργασία

Σχεδιασμός συστήματος μέτρησης ταλαντώσεων για τη γέφυρα του Μετσόβου

υπό

Κωνσταντίνου Αργύρη

Διπλωματούχου Μηχανολόγου Μηχανικού, Π.Θ., 2011

Υπεβλήθη για την εκπλήρωση μέρους των
απαιτήσεων για την απόκτηση του
Μεταπτυχιακού Διπλώματος Ειδίκευσης

2013

Το έργο υλοποιείται στο πλαίσιο της Πράξης «ΑΡΙΣΤΕΙΑ» του Επιχειρησιακού Προγράμματος «Εκπαίδευση και Δια Βίου Μάθηση» και συγχρηματοδοτείται από την Ευρωπαϊκή Ένωση (Ευρωπαϊκό Κοινωνικό Ταμείο-ΕΚΤ) και από εθνικούς πόρους.

Εγκρίθηκε από τα Μέλη της Τριμελούς Εξεταστικής Επιτροπής :

Πρώτος Εξεταστής (Επιβλέπων)	Δρ. Κωνσταντίνος Παπαδημητρίου Καθηγητής, Τμήμα Μηχανολόγων Μηχανικών Πανεπιστήμιο Θεσσαλίας
Δεύτερος Εξεταστής	Δρ. Κερμανίδης Αλέξης Επίκουρος Καθηγητής, Τμήμα Μηχανολόγων Μηχανικών Πανεπιστήμιο Θεσσαλίας
Τρίτος Εξεταστής	Δρ. Τσόπελας Παναγιώτης Καθηγητής, Τμήμα Πολιτικών Μηχανικών Πανεπιστήμιο Θεσσαλίας

Ευχαριστίες

Πρώτα απ΄ ολα, θα ήθελα να ευχαριστήσω τον επιβλέποντα της μεταπτυχιακής εργασίας μου, Καθηγητή κ. Παπαδημητρίου Κωνσταντίνο, για την πολύτιμη βοήθεια και καθοδήγησή του κατά τη διάρκεια της συνεργασίας μας. Επίσης, ευχαριστώ τα υπόλοιπα μέλη της εξεταστικής επιτροπής της μεταπτυχιακής εργασίας μου, Καθηγητές κ. Κερμανίδη Αλέξη και κ. Τσόπελα Παναγιώτη για την προσεκτική ανάγνωση της εργασίας μου και για τις πολύτιμες υποδείξεις τους. Πάνω απ' όλα, είμαι ευγνώμων στους γονείς μου, Γιώργο και Σεβαστή για την ολόψυχη αγάπη και υπομονή τους όλα αυτά τα χρόνια καθώς και για τη υποστήριξη που μου έδωσαν να συνεχίσω τις σπουδές μου.

Κωνσταντίνος Αργύρης

Abstract

This thesis addresses the issue of designing a vibration measurement system for large structures. The system is demonstrated for the ravine bridge of Metsovo. This work presents a complete approach covering all major subjects of vibration measurement, from the equipment to the methods of data collection. A thorough description of a new measurement system available in the System Dynamics Laboratory, and its capabilities are presented. The instruments of the System Dynamics Laboratory have many new features compared with older instruments and this provides the designer with many options. The reader is exposed to these features in the most sensible manner, in order to be able to use the instruments properly and exploit their full capabilities.

The theoretical (FEM) model of the Metsovo Bridge is presented, and it is explained why it is an important part of the measurement process. Next, the topic of Modal Analysis is discussed, and Operational Modal Analysis theory is briefly presented. This part is responsible for extracting the modal properties of the structure from ambient vibration measurements.

The issue of mode shape assembly is addressed, which is common when dealing with large structures like bridges or buildings. The main theme here arises from the fact that the larger the structure is, the more points (DOFs) must be measured in order to obtain an accurate view of the mode shapes. But due to the limited number of sensors or practical issues, not all DOFs can be measured at the same time. Therefore we must perform sequential measurements in different DOFs each time. However, a certain number of sensors must remain in the same positions, while the rest are moved throughout the entire span of the structure. The former are called 'reference sensors' while the later are called 'moving sensors'. In this work, the issue of taking into account all the measurements in different positions taken from different sensor configurations is addressed.

The issue of optimizing the location of the reference sensors is also addressed. The locations where we place our sensors is very important because it can affect the quality of the measured data. Two methods are proposed for finding the optimal sensor location, one empirical, and one more sophisticated, based on information entropy.

Contents

1 Introduction **2**
- 1.1 Overview of Operational Modal Analysis . . . 4
- 1.2 Overview of Mode Shape Assembly . . . 6
- 1.3 Overview of Optimal Sensor Location . . . 7

2 The measurement equipment **9**
- 2.1 General information . . . 9
- 2.2 The MR3000 in more detail . . . 11
- 2.3 Communication with the MR . . . 14
- 2.4 Configuring the MR . . . 21
- 2.5 The accelerometers . . . 25
- 2.6 Connection Examples . . . 27
- 2.7 Convenience issues - Sensor Units . . . 30

3 Theoretical model of the Metsovo Bridge **31**
- 3.1 Description of the Metsovo Bridge . . . 31
- 3.2 Finite Element Model of the Metsovo Bridge . . . 34

4 Modal Analysis **49**
- 4.1 Operational Modal Analysis . . . 50

5 Mode Shape Assembly **54**
- 5.1 Problem description . . . 54
- 5.2 Proposed methodology . . . 55

6 Optimal Sensor Location **59**
- 6.1 Visual Inspection Method . . . 59
- 6.2 Information Entropy Method . . . 63

7 Conclusions **76**

Chapter 1

Introduction

During the last decade modal analysis has become a key technology in structural dynamics analysis. Starting from simple techniques for trouble shooting, it has evolved to an established technique to analyze the dynamical behavior of complex mechanical structures. Beginning from the modal model, design improvements can be predicted and the structure can be optimized. Based on the academic principles of system identification, experimental modal analysis helps the engineers to get more physical insight from the identified models. Continuously expanding its application base, modal analysis is today successfully applied in civil engineering (buildings, bridges, off-shore platforms, dams), automotive engineering (engine, suspension, fully trimmed cars), aircraft engineering (in-flight tests, ground vibration tests, landing gear, control surfaces), spacecraft engineering (launchers, antennas, solid panels, satellites) and industrial machinery (pumps, compressors, turbines).

A great number of structures require certain specifications for safe and precise operation conditions, which usually form the most significant design parameters. In order to ensure a constantly accepted and reliable performance of a system, the knowledge of its dynamic behavior becomes essential in either case of operational or unpredictable extreme loads. For newly build structures, as well as for the ones that are already in operation for some time, the measurement of their dynamic properties, such as natural frequencies, damping factors and modeshapes is well desired, so as for the prediction of their behavior using a reliable model to be feasible.

The vibration of a structure originates from its resonance modes that are inherent properties of the structure. Small forces exciting the structure at one or more of these resonance frequencies can cause large vibration responses resulting in possible damage, discomfort and malfunctioning in the structure. These modes are determined by the geometry, the material properties (mass, damping and stiffness) and the boundary conditions of the structure. If the geometry, material properties or boundary conditions change, the structural modes change.

The modal model expresses the behavior of a linear time-invariant mechanical system as a linear combination of these different resonance modes. Each mode is defined

by a damped resonance frequency, modal damping and mode shape, i.e. the so-called modal parameters. Given the physical interpretation of the modes, engineers often prefer this mathematical model because it provides the best physical understanding for the system.

Experimental modal analysis (EMA) identifies a modal model from the measured forces applied to the test structure and the measured vibration responses. Classically, one applies an artificial, measurable input to the system and one measures the output. From these measurements, the experimental model can be obtained by a variety of parameter estimation methods. During an EMA, the structure is often removed from its operating environment and tested in laboratory conditions.

The latter experimental situation can differ significantly from the real-life operating conditions. Cases exist where it is rather difficult to apply an artificial force on a structure and one has to rely on available ambient excitation sources. For these cases, system identification techniques were developed to identify the modal model from the structure under its operational conditions from vibration responses only. These techniques, referred as operational modal analysis (OMA) or output-only modal analysis, take advantage of the ambient excitation as e.g. wind, traffic and turbulence. OMA proved very useful in civil engineering, where it is very difficult and expensive to excite constructions such as bridges and buildings with a hammer or shaker and to obtain artificially induced vibration levels that exceed the natural vibrations due to traffic or wind. In mechanical engineering, OMA is successfully applied to obtain data-based dynamic models of, for instance, a vehicle during road testing or an aircraft during flight tests. Also, an important advantage of OMA is that the structure can remain in its normal operating condition. This allows the identification of more realistic modal models for in-operation structures.

There are certain limitations in the effectiveness and reliability of the modal model identification techniques. These limitations are summarized as follows.

Insufficient measurement data: This is due to the limited number of sensors placed in the structure. As a result only estimates of the partial modeshape of the structure are available at the measured degrees of freedom (DOF). Also, this is due to the usually limited range of the frequency band contained in the excitations forces that, as a result do not excite all modes of the structure and therefore some of the system's dynamic properties cannot be identified. The problem is more pronounced with the higher frequency modes since, from a testing point of view, it is more difficult to excite the higher frequency response of a structure since more energy is required to produce measurable response at these higher frequencies than at the lower frequencies. It should be noted that optimal sensor location strategies could be used to give the best possible information about the modes of the excited system.

Measurement error: These are errors associated with the dynamic data measurements. It consists of bias errors caused by faulty instruments or noise caused by changes in the environmental conditions during testing or poor preprocessing of the initial data (for example, bias from windowing of the data). The effect of noise on

the modal identification results is that it limits the number of modes that can be estimated reliably. This is more pronounced for higher modes where the signal-to-noise ratio is relatively small. Thus, often the modal parameters can be identified only for the dominant modes in the measurement records.

Modal coupling: It is often difficult to identify the closely spaced modes which are contributing to the measured response within the measured frequency range of interest. This difficulty is observed more commonly at the higher frequency portions of the spectrum where the modal density is typically greater.

Non-uniqueness: This is due to the fact that the number of parameters is larger than needed or the available measurements are relatively limited. In such case, the optimal solution to the identification problem appears not to be unique.

Ill-Conditioning: This is due to the lack of sensitivity of the measurement quantities to small changes in the modal parameters to be identified.

Model Error: This is due to the fact that the chosen class of linear modal models chosen for identification is unable to exactly model the actual behavior of the structure (for example, due to nonlinear behavior of the structure at a portion of the frequency range).

1.1 Overview of Operational Modal Analysis

The peak-picking method is the simplest method to estimate the modal parameters of a structure subjected to ambient loading. It is based on the power spectra that are obtained from the measured time histories using discrete Fourier transform. The locations of the peaks of the power spectra give an estimate of the modal frequencies. The mode shapes are determined by computing the cross power spectral density functions between all outputs and a reference sensor. The method requires that the damping is low and the modes are well-separated. Violation of these two assumptions may lead to erroneous results. A disadvantage of the method is the subjective selection of modal frequencies and the lack of accurate damping estimates. However, the major advantage of the method is its speed. In general, the method identifies the operational deflection shapes instead of mode shapes, since there is no modal model that is fitted to the measured data. In particular, for the case of closely spaced modes such operational deflection shapes will be the superposition of the modeshapes of the multiple closely-spaced modes.

Statistical methods for the estimation of the modal parameters based on output-only measurements have been proposed. Frequency-domain maximum likelihood approaches for the estimation of modal parameters from output-only data were proposed by Hermans et al. (1998). A Bayesian statistical approach for modal identification has also been proposed by Katafygiotis and Yuen (2001) using ambient data. The method is based on the statistics of an estimator of the spectral density. This approach allows for the direct calculation of the probability density functions (PDF) of

the modal parameters which can then be approximated by an appropriately selected multi-variant Gaussian distribution.

Besides the aforementioned modal identification approaches, several methods proposed are based on fitting directly the measured data with modal model predicted data using least-squares type of approaches. In Beck et al. (1994) a methodology for modal identification is proposed using time-domain least-squares methods based on correlation functions of the output time histories. In Brinker et al. (2001), frequency-domain least-squares methods based on full cross-power spectral densities (CPSD) are proposed. Finally, Peeters and Van der Auweraer (2005) have proposed a frequency-domain least-squares modal identification methods based on half spectra.

There are certain advantages for using output only measurements for identifying the structural modes. In operational modal analysis there is no need to use artificial devises for exciting the structure. Instead, the modes are identified from the vibrations obtained during the operation of the structure. This has certain advantages for massive civil structures for which large exciters have to be used to excite the structure. The use of exciters is not only very costly but it is also time-consuming and impractical for structural health monitoring applications. Ambient vibration measurement can directly be used for continuously monitoring the civil engineering structures. Finally, it is worth noting that the OMA methods provide the modal properties that correspond to the real operation conditions of the structure. These conditions may differ significantly from the ones obtained during laboratory forced excitation tests. Examples of this situation include the modal properties obtained for bridges using large exciters. Such modal analyses are usually performed under closed traffic conditions. For bridges that are open in traffic, one should expect changes in mass loading due to the vehicles passing through the bridge. These changes alter the modal properties of the structure.

The disadvantages of the operational modal analysis methods are the broadband assumptions on the unknown input and the low signal to noise ratios for the low level vibrations on which usually the measurements are made. In particular, all operational modal analysis methods are based on the fact that the unknown input forces can be adequately modeled by white noise processes. This condition is often violated since excitation forces may contain harmonic components which will appear as peaks in the spectra and may be erroneously identified by the methods as structural modes.

1.2 Overview of Mode Shape Assembly

Modal identification involves the determination of natural frequencies, damping ratios and modeshapes from measured vibration data of the structure in its constructed state. Attributed to advances in sensing technology and identification methods, full-scale tests have become a feasible option for assessing the actual dynamic properties of structures. Besides natural frequency and damping ratios, mode shapes identified from vibration tests provide insights into the nature of modes through relative motions at the measured degrees-of-freedom (DOFs) of the structure. While modern sensing and data acquisition technology have allowed high resolution time history data to be obtained, the spatial resolution of mode shape can only be improved by increasing the number of sensing locations. Due to limited instrumentation budget and practical difficulties in deploying a large array of sensors with synchronous data acquisition, full mode shapes with a large number of measured DOFs are often assembled from partial (local) ones identified from individual setups, each covering a different part of the structure. Since the modeshapes identified from individual setups are arbitrary in sense and scaling, common 'reference' s must be present across different setups in order to allow their modeshapes to be assembled. The reference DOFs must have significant frequency response in the modes of interest. There must also be at least one common reference DOF across any two setups.

Incorporating information from different setups in a consistent manner to form the overall mode shape is not always trivial. In general, some DOFs may be measured by more than one channel in the same setup. There are also reference DOFs measured in more than one setup. Mode shapes identified from different setups are normalized individually and they can have different sense (i.e., signs). They must be scaled properly to form an overall shape, but the scaling factors are unknown beforehand and therefore must be calculated.

Chapter 5 develops a theory with an automated procedure for assembling mode shapes in a general context that addresses the aforementioned issues. The optimal mode shape is formulated as the one that minimizes an objective function. The latter is formulated to properly account for the discrepancy between the theoretical and identified mode shapes.

1.3 Overview of Optimal Sensor Location

Chapter 6 deals with the issue of finding the optimal locations for our reference sensors. It presents two methods for approaching the problem. The first relies on visual inspection of the mode shapes of the structure as they are predicted by the FEM model. The second is much more involved and makes use of the Information Entropy.

The problem of parameter estimation of structural models using measured dynamic data is important in modal identification, structural model updating, structural health monitoring and structural control. The estimate of the parameter values involves uncertainties that are due to limitations of the mathematical models used to represent the behavior of the real structure, the presence of measurement error in the data and insufficient excitation and response bandwidth. In particular, the quality of information that can be extracted from the data for estimating the model parameters depends on the number and location of sensors in the structure as well as on the type and size of model and measurement error. The objective in an experimental design is to make a cost-effective selection of the optimal number and location of sensors such that the resulting measured data are most informative for estimating the parameters of a mathematical model of the structure.

Information theory based approaches have been developed to provide rational solutions to several issues encountered in the problem of selecting the optimal sensor configuration for modal identification and structural parameter estimation. The optimal sensor configuration is selected as the one that maximizes some norm (determinant or trace) of the Fisher information matrix (FIM). The information entropy, measuring the uncertainty in the model parameter estimates, was also introduced for designing optimal sensor configurations. It was shown that, asymptotically for very large number of data, the information entropy depends on the determinant of the FIM, justifying the use of the determinant instead of the trace or other scalar measures of FIM in previous approaches. The information entropy has been applied to design optimal sensor locations for parameter estimation using ambient vibrations, model class selection for damage detection, as well as to design the optimal excitation characteristics (e.g. amplitude and frequency content) for the identification of linear and strongly nonlinear models.

The optimal sensor location problem is formulated as a single-objective optimization problem involving discrete-valued variables. Computational efficient algorithms for solving the discrete-valued minimization problem have been proposed. Udwadia (1994) demonstrated that using the trace of the FIM is computationally very attractive since the solution of the underlined discrete optimization problem is straightforward. However, for other more popular scalar measures of uncertainties such as the determinant of the FIM or the information entropy, an exhaustive search over all possible sensor configurations is required to obtain the exact optimal sensor configuration. This approach is computationally prohibitive even for structures with a relatively small number of degrees of freedom (DOFs). Heuristic optimization tools have also

been developed as effective alternatives for efficiently solving these discrete optimization problems involving discrete-valued variables. Exploiting theoretical asymptotic results on information entropy and FIM, two computationally efficient heuristic algorithms, the forward sequential sensor placement (FSSP) and the backward sequential sensor placement (BSSP) were proposed by C. Papadimitriou (2004, 2005). These algorithms construct sensor configurations for physical model parameter estimation, corresponding to information entropy values very close to lower or upper bounds of the information entropy. The numerical results indicated that the proposed heuristic algorithms provide sub-optimal sensor configurations that can be extremely good approximations of the optimal sensor configuration [C. Papadimitriou 2004, 2005]. Moreover, these heuristic algorithms are very simple to implement in software and computationally very efficient.

In most information theory-based methods the effect of spatially correlated prediction errors and its importance was not adequately explored. The present study provides insight into the effect of spatially correlated prediction errors on the design of the optimal sensor locations. The information entropy is used as the performance measure of a sensor configuration. The information entropy is built from the parameter uncertainty identified by applying a Bayesian identification framework. The optimal sensor location problem is formulated as a single-objective optimization problem involving discrete-valued variables. The effectiveness of available heuristic algorithms BSSP and FSSP, known to be computationally very efficient and accurate for uncorrelated prediction errors, is explored.

Asymptotic approximations, valid for large number of data, available for the information entropy [C. Papadimitriou 2004] for the case of uncorrelated prediction errors are extended to account for the case of spatially correlated prediction errors. Useful theoretical results are derived that show that the lower and upper bounds of the asymptotic estimate of the information entropy, corresponding, respectively, to the optimal and worst sensor configuration, are a decreasing function of the number of sensors. In addition, it is shown that for up to the characteristic length of the highest contributing mode of the structure, the spatial correlation between prediction errors forces the minimum distance between sensors to be of the order of the prediction error correlation length. Consequently, sensor placement becomes independent of the mesh size of the finite element models used for structural dynamics simulations. For distances between two sensors higher than the characteristic length, the sensor locations are affected also by the spatial variability of the response sensitivities computed by a nominal structural model. Implementation in structural dynamics is concentrated on the design of optimal sensor location for (a) modal identification and (b) estimation of structural model (e.g. finite element) parameters. Theoretical and computational developments are demonstrated by designing the optimal sensor configurations for the finite element model of the Metsovo Bridge. It is illustrated that the extent of the spatial correlation of the prediction errors has an important effect on the optimal sensor locations. In addition, inadequacies of the spatially uncorrelated prediction error models are emphasized.

Chapter 2

The measurement equipment

2.1 General information

In this section we present a basic description of the measurement equipment that is available in the System Dynamics Laboratory to carry out the field measurements.

2.1.1 Overview

This section provides a basic overview of the measurement equipment and its capabilities. The following sections provide more details about each specific part of the system.

The measurement system used is the MR3000 by SYSCOM Instruments. The MR3000 is a new family of compact vibration and motion measurement system. As such it meets all user expectations in a state-of-the-art device and thus is a highly reliable and efficient instrument for various application fields.

It is equipped with a newest generation of electronic components, which allows a strong reduction in power consumption while increasing the computing power. On the firmware side, the MR3000 has a built-in FTP client and server to exchange the data and a built-in Web server to configure the device via the WebUI (Web based user interface).

No special hardware or software is needed to communicate with the MR3000 - any device with a Web browser and Internet connectivity (such as Smartphones, Tablet-PCs or Laptops) will work. The user can set-up the unit, download files via any type of connection (wired, wireless or GPRS). In addition, a real-time data-stream from the recorder to a FTP-server is implemented. The alerting feature of the MR3000 enables it to automatically send alarm messages via SMS message or e-mail to warn the analyst about potentially dangerous or unwanted vibration levels.

The measurement data is stored in a standard SD-Flashcard and managed by a linux-type file-system. The initial capacity is 4 gigabytes, but the user can easily install an SD-Flashcard of larger capacity if the instrument is intended for long measurement sessions.

The MR3000 is pre-configured for the use with internet or external sensor. In the context of this thesis, all measurements were performed using external sensors (accelerometers). The sensors can be uniaxial or triaxial. The triaxial sensors are composed of 3 orthogonally oriented uniaxial sensors and can measure the acceleration at a specific point in all 3 directions (X,Y,Z). The sensors pick up the vibration and transform it into an electrical signal (analog) which is proportional to the acceleration. The signals of the sensors are continuously digitalized and stored in the ring-buffer memory. If the vibration exceeds the threshold level (trigger criteria are fulfilled) or if we used manual recording, the content of the ring-buffer memory is written to the internal SD-Flashcard from where it can be easily transferred to a device with network connectivity (laptop, smartphone,tablet pc) and analyzed.

The MR3000 may optionally be equipped with an external GPS antenna for a precise timing, but there are also other ways to synchronize the instruments which will be covered in more detail in the next sections.

The MR3000 is water and shock resistant. An external rechargeable lead-acid battery ensures continuous operation during power interruptions. In general, the MR is easy to operate and requires minimal maintenance. Routine maintenance and operation does not require a specialist.

2.1.2 Features

Major features include :

- Compact unit with digital recorder, wired and wireless connectivity
- Up to 32GB memory
- Integrated Web server
- Precise timing, GPS is optional
- Power over Ethernet (PoE, explained in greater detail in the later section)
- Wide dynamic WiFi range (132dB) for wireless connection
- Sampling rates up to 1kHz
- Simple installation
- Easy operation
- High reliability
- Low maintenance

2.1.3 Applications

The MR3000 can be used for vibration and motion measurement in various fields such as :

- Civil Engineering
  - Industrial Vibrations
  - Construction Site Monitoring
  - Tunneling
  - Truck and Rail Traffic
  - Blasting Monitoring
  - Model Verification
- Earthquake Engineering
  - Building Monitoring
  - Monitoring of Structures (e.g. Dams, Bridges)
- Geology
  - Soil Characterization
- Earth Science
  - Earthquake Monitoring

2.2 The MR3000 in more detail

The MR3000 Motion Recorder is the most basic unit of the system, in the sense that it is the only unit that the user interacts with, so all the settings for each specific measurement have to be done through the MR. This section will present a more detailed view of the MR and its characteristics.

2.2.1 Hardware

In the next figure we see a mechanical drawing of the MR, and the explanation right below.

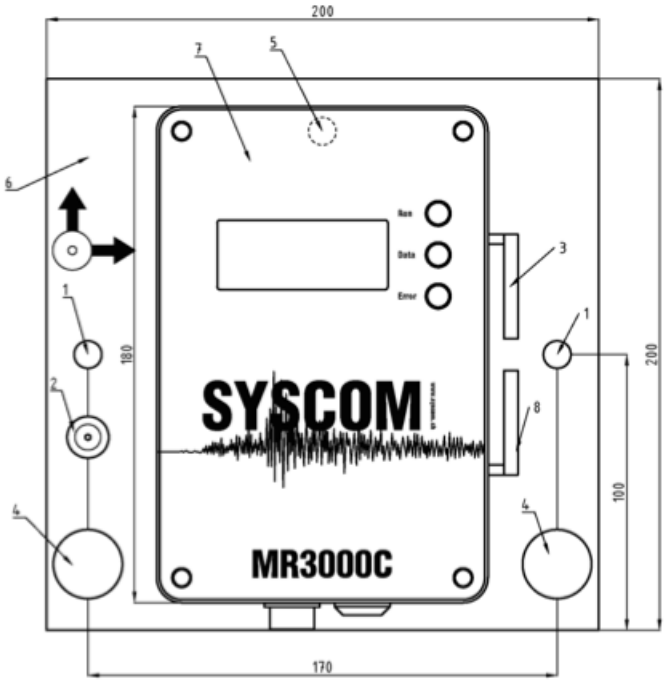

Figure 2.1: Mechanical drawing of the MR3000 - Top View

1. Fixation of the mounting plate
2. Bubble level
3. WiFi antenna
4. Knurled screw
5. Knurled screw - below MR
6. Mounting plate
7. Lid
8. GSM antenna

In the next figure we see the side view of the MR.

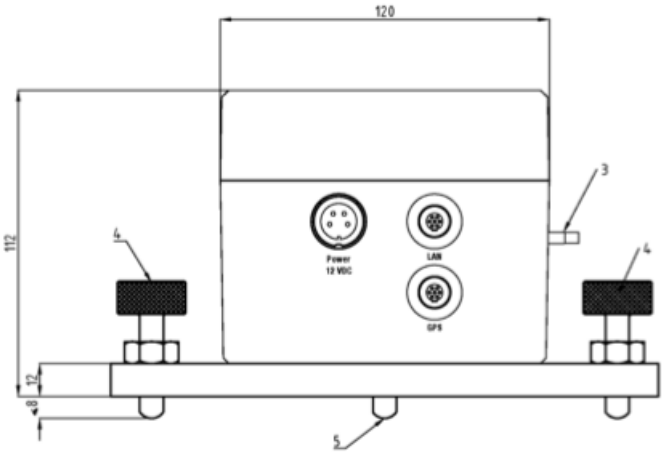

Figure 2.2: Mechanical drawing of the MR3000 - Side View

2.2.2 Connectors

The MR3000 provides three push-pull connectors, as it is shown in Figure 2.2 above, namely, **Power** for power supply, **LAN** for communication and power using PoE (Power over Ethernet), and **GPS** to connect an external GPS antenna. The LAN port is also referred to as the **Ethernet** port.

Power

Here we connect either an external AC/DC adapter, or the battery pack supplied with the MR3000.

NOTE: There is no internal battery in the MR3000.

LAN

Here we connect the Ethernet cable for wired communication via router or direct connection to a PC. Each connection will be examined in more detail in section 2.3. The important thing to note is that if we connect the MR to a router (or switch) with PoE capabilities, the MR is powered over this connection and no additional power supply is needed. Still, it is considered good practice to connect an additional power source for redundancy.

GPS

Here we connect an appropriate GPS module for the most accurate time synchronization.

2.2.3 Battery pack

The MR3000 comes with an external lead-acid gel cell battery (5Ah) with integrated AC battery charger. The battery pack is very important because it is the only way of powering our MRs when we are performing measurements out in a field where there is no power supply. If there is a power supply, we can still use the battery pack and connect it to the power supply so that the battery will not die out and ensure continuous operation in the case of a power shutdown.

Figure 2.3: The external battery pack with integrated charger

2.3 Communication with the MR

To communicate with the MR3000 there is no need for any special software, any Web browser will work. Generally, there are two ways of communicating with the instrument. Direct and in-direct.

2.3.1 Direct connection

In direct connections our computer can talk to the instrument directly, meaning that they belong to the same network and subnet. Devices that are in the same subnet can talk to each other directly without the traffic passing through any other computer/server. To establish a network device (such as the MR, a laptop etc) in the same subnet as another network device we must make sure that these two devices have the same *IP Address* and *Subnet Mask*. There are two ways to assign these parameters to a networking device. Automatic (DHCP) and manual.

Automatic

This method uses a DHCP (Dynamic Host Controller Protocol) server. A DHCP server is installed by default in nearly all *routers* and its job is to automatically assign IP Addresses to devices that request one. It is the DHCP server's job to make sure that the IP Addresses assigned are on the same subnet so that the devices can communicate. In this case, if a router is available, all the user has to do is to run an ethernet cable from the MR to one of the routers ports. The MR is pre-configured to send DHCP requests when a cable connection is made, then these requests will be picked up by the router and it will take care of the rest. In exactly the same way the user can connect multiple MRs. When the instrument(s) finally obtain the IP Address, it will be shown in the display so that the user can read it. This is necessary because if we don't know the IP Address of the instrument we don't know what to type in the Web Browser to communicate with it. Of course, our computer must be connected to the same router, and the same procedure applies to it as well. An important detail is that most routers have WiFi antennas. This enables the laptop to connect to the router wirelessly, and thus limits the amount of cable needed and enhances the portability of the laptop which will not have a cable attached to it. [1]

In the next figures we see how a common router looks like, and a sketch showing the network setup under discussion.

Figure 2.4: A common TP-Link router with WiFi antenna

[1] Only the computer can connect wirelessly to the router, **not** the MRs.

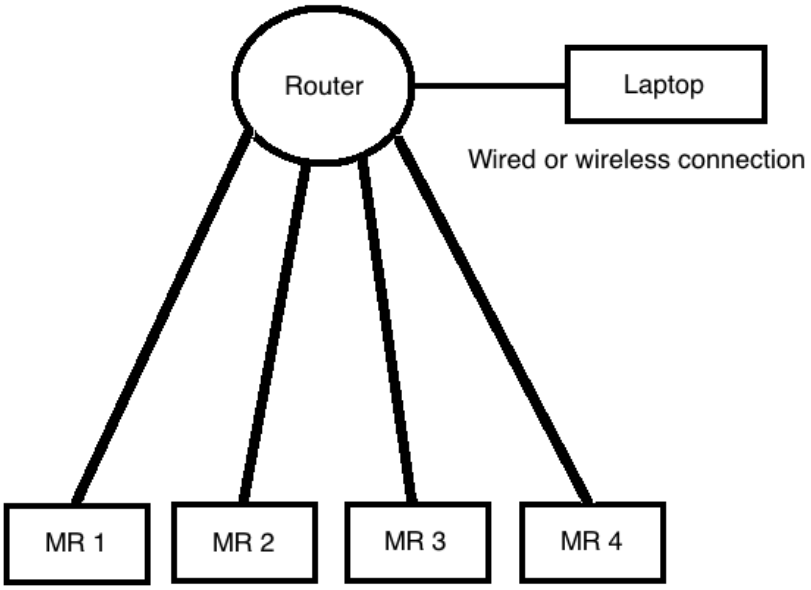

Figure 2.5: Direct wired connection via Router

The important thing to note here is the presence of the DHCP server provided by the router. Whereas nearly all routers nowadays have a DHCP server pre-installed, switches (in general) do not. So if a switch is available instead of a router we can not have automatic IP Address assigning and this leads us to the manual assigning which will be described in the next paragraph.

A final note about the router, is that if it provides PoE (Power over Ethernet) capabilities, the MR can be powered through the same cable and there is no need for another power source such as the battery or the AC/DC adapter. On the other hand, routers with PoE capabilities are not common and usually they are very expensive as well. So if we want to use PoE, the usual way is to use a switch. The switch can be used in conjunction with the router just to provide its PoE capabilities, while we keep the routers advantages as well.

Manual

As it was previously mentioned, automatic IP Address assigning happens only when there is a router present in the network. There are two situations in the wired connection case where this is not the case. The first is when we use a switch to establish the instruments and the computer in the same network, and the second is when we connect the instrument directly to the computer. Obviously, in the latter case we can only talk to one MR at a time.

In these cases we have to manually assign an IP address to *each one* of the instruments *and* the computer. We also have to make sure that these IP addresses belong in the same subnet as well, so that the devices can communicate. The way to do that is by adjusting the networking properties of the MR and the computer. The MR's networking properties can be changed from it's WebUI rather easily from the *User Parameters - Ethernet* tab. We just have to set a *Static* IP Address, i.e. 192.168.1.2, and leave the subnet mask as it is (255.255.255.0). The subnet mask should remain unchanged and will work most of the time. Changing the subnet mask is required in very rare situations and does require en expert. We do the same procedure in all the MRs we would like to use and assign a *different* IP Address to each one but we change only the last digit and make sure the subnet mask is the same. For example the second MR could have the IP Address 192.168.1.3 and subnet mask 255.255.255.0 and so on.

Obviously, in order to be able to view the WebUI we must already be connected to the MR. The usual way is to first configure the instruments in the lab where there is a router present and save the changes. If there is no router present we can connect wirelessly to the MR and configure it.[2] The wireless connection will be examined in a seperate paragraph.

The final step is to configure the computer to use a static IP Address instead of trying to obtain a dynamic one from DHCP. The exact steps to do that depend on the operating system of the computer, but in general we have to navigate to the Control Panel - Network Adapters and change the properties of the ethernet adapter from dynamic to static. The static IP Address should also be in the form 192.168.1.x where x is a number **not** assigned to **any** MR, and the subnet mask should be the same (255.255.255.0). The following figures demonstrate this procedure in a Windows 7 machine.

[2]In this case we can only talk to one MR at a time.

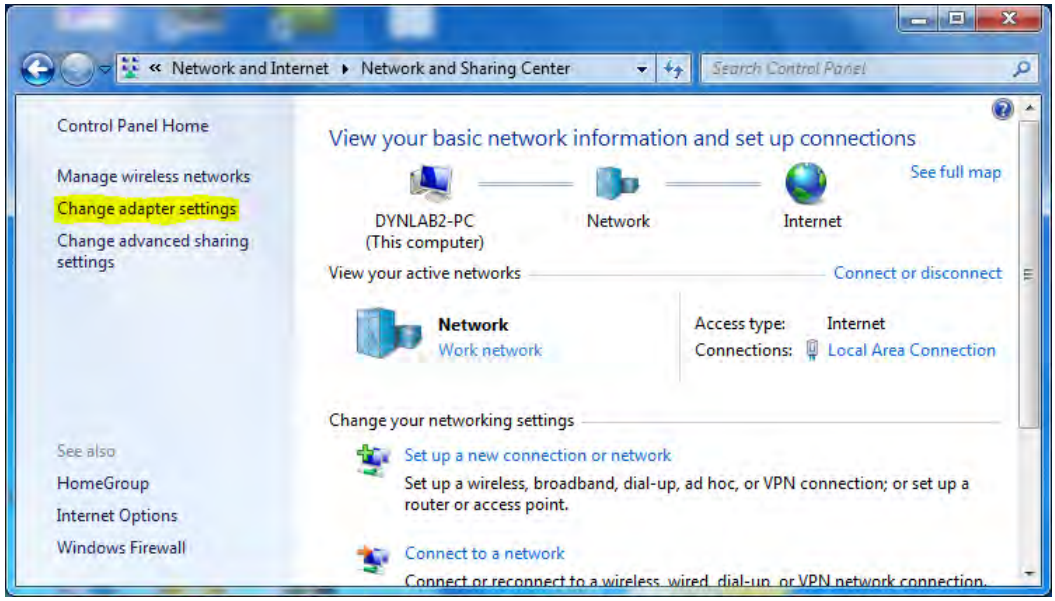

Figure 2.6: Static IP Address assigning to a Windows 7 machine

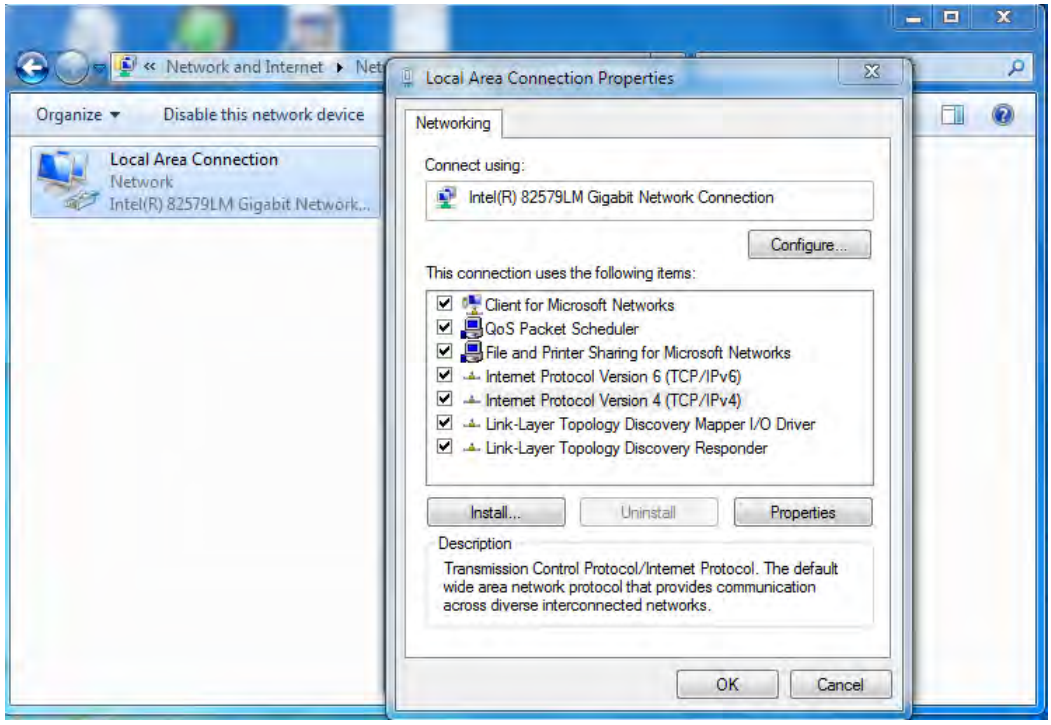

Figure 2.7: Static IP Address assigning to a Windows 7 machine

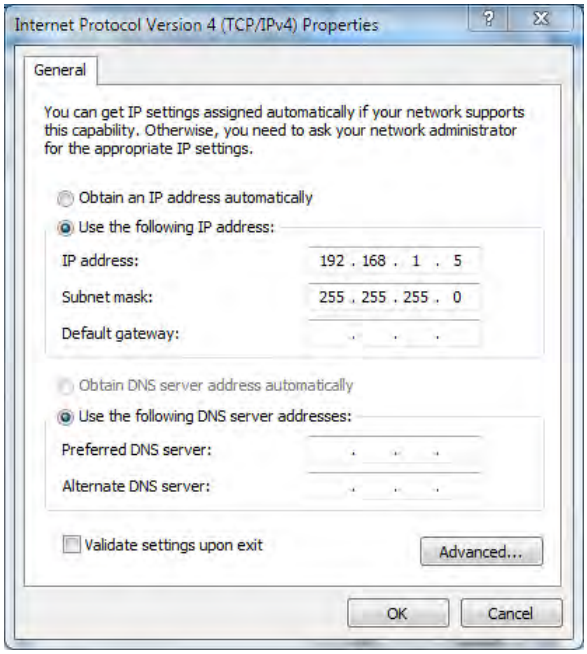

Figure 2.8: Static IP Address assigning to a Windows 7 machine

The fields Default Gateway and DNS Servers are needed only in the case where there is a router with an active internet connection in the network (the *Automatic* case). In the manual case we can leave these fields blank.

After we have correctly assigned IP Addresses in the same subnet in all the MRs and the computer, we can connect them directly to a switch using standard ethernet cables (RJ45). If the switch has PoE capabilities, the MRs can also be powered from the same cable. Alternatively, if there is no switch, we can connect the MR directly to the computers ethernet adapter. In both cases, after the connection is successfull, we just have to open our web browser of choice and enter the IP Address of the MR we would like to configure. In the case where everything is connected to a switch, it is possible to open multiple tabs in the web browser (one for each MR) and configure them at the same time. In the case where we have the instrument connected directly to our computer, we can only type the specific instruments IP Address in the web browser and configure one at a time. In the following figure we see the switch used in the lab. It is a PoE switch with 16 ports half of which have PoE capabilities.

Figure 2.9: Cisco switch with 16 ports and PoE capabilities

If PoE is desired we connect our cable(s) to one of the PoE ports. Care needs to be taken here regarding the power consumption of the switch. The switch shown above uses a 48V AC/DC power adapter and can consume up to 120 Watts of power. The reason for such a high power consumption (compared to a typical switch which consumes roughly 10 Watts) is the Power over Ethernet feature it provides. We must also remember that in a electric cable the loss of power is proportional to the distance of the cable. So if we want to have long ethernet cables because for example we are measuring vibrations at a large structure, we must have the ability to provide more power in order to compensate for the loss due to the increased length. This is an important factor if we are out in the field with no external power supply, because using the switch to its full power with long cables could drain our batteries or generator more quickly. If that is the case, it is a more safe solution to power the instruments with their batteries instead of PoE, and use the ethernet cables just for networking purposes (non-PoE ports).

2.3.2 Wireless connection

There is also the possibility of connecting wirelessly to the MR. In that case the MR acts as an access-point to which other computers can connect. The advantage of this method is that there are no cables involved at all and there are no limitations regarding the positions of the instruments in the field. Each one acts independent from the others and transmits its own WiFi signal. The MR starts to transmit this signal as soon as it is powered on (unless the user has disabled it from the WebUI) and it can be picked up by any laptop with a WiFi antenna. The name of the WiFi network is the serial number of the specific instrument so we know which signal corresponds to which instrument. After we have connected to the wireless network of

the MR we open our browser and type the IP Address 192.168.30.1. This IP Address is always the same and should not be confused with the one that the instrument obtains through wired connection. After we have pointed our browser to this address we meet the WebUI exactly as in the case of the wired connection.

The disadvantage of the wireless connection is that we can only be connected to one instrument at a time. We must also have visual contact with the instrument in order to receive the transmited signal with adequate strength. For that reason the WiFi antenna of the instrument (part 3 in figure 2.1) should not be kept in a closed, confined space.

2.3.3 In-direct connection

In in-direct connections our computer reaches the MR through another server on the internet using VPN (=Virtual Private Network). This method enables the user to connect to the MR from virtually anywhere provided that both the MR and the user have active Internet connections. VPN is of practical interest in cases where we have installed a permanent sensor network in a structure and we would like to periodically obtain the measurement data or configure the instruments. The basic difficulty here is that in most field measurements there is no active internet connection, and VPN can not work without the internet. If the MR is online, we can configure it from its WebUI to use VPN, and it will asssign a virtual IP Address to itself. We can connect to that address from any computer with an internet connection through a VPN client after we provide the username and the password that we have chosen. Then VPN will simulate the local network of the MR, and our remote computer will behave as if it was in the same network too.

2.4 Configuring the MR

After we have successfully connected to the instrument(s) with one of the methods described in the previous section, the next step is to configure them. Configuration includes specifying the parameters of the instrument such as the time synchronization, sampling rate, recording type, trigger levels etc. All the configuration is done from the Web User Interface.

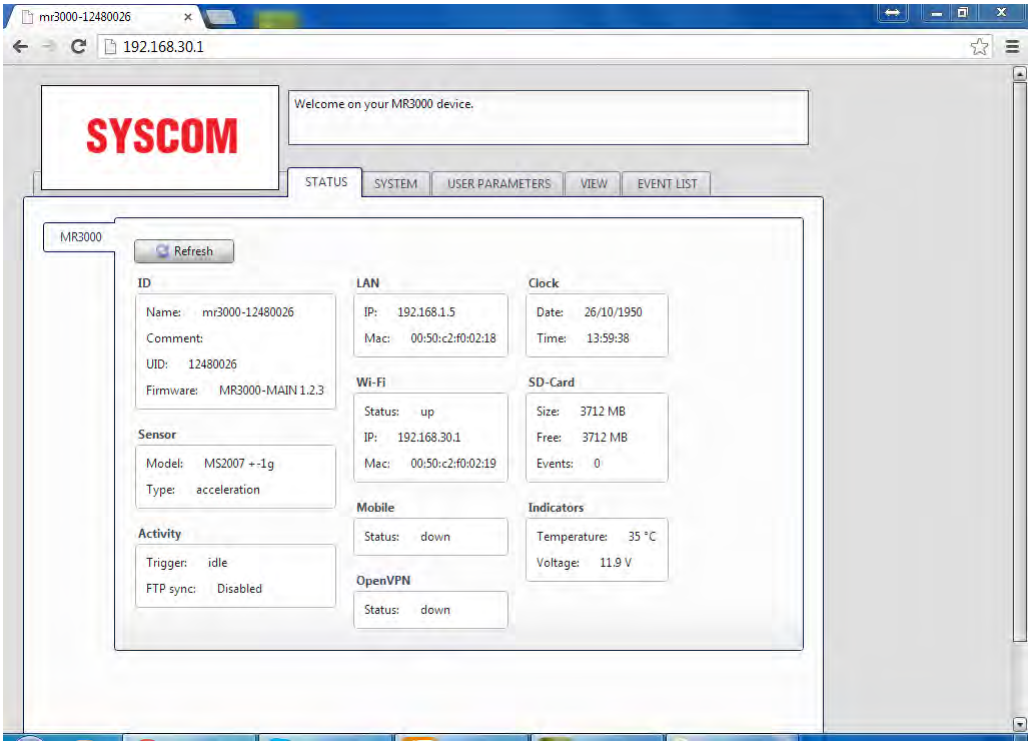

Figure 2.10: The Web User Interface

In the *Status* tab we can view all the basic settings such as the time, available capacity, recording status etc. The *System* and *User Parameters* tabs enable us to modify the instruments settings according to our needs and goals. The most important tabs are listed below along with a description.

2.4.1 System - Time

This tab enables us to choose between 3 time synchronization modes. Manual, Network, and GPS.

In **Manual** mode we specify a time and date and the MR keeps it using its internal clock. So we do not have *continuous* update of the time. However, electronic components involved in timekeeping always have a drift, depending on unpredictable factors like temperature. As a consequence the MR will slowly drift away from the right time.

In **Network** synchronization the clock will be *continuously* synchronized using a NTP (Network Time Protocol) server that is defined with its IP address. The accuracy depends on the quality of the internet connection and on the distance from the server. The closer we are on a NTP server the better accuracy we will have.

Typical accuracy on the Internet ranges from 5ms to 100ms. If the NTP server is on the Internet outside of our local network we will need an Internet connection in order to reach it. If it is in our local network we do not need an internet connection and we just have to enter its local IP address. This is the case in the master-slave configuration which will be presented in the next section.

In **GPS** synchronization the clock is *continuously* synchronized with the GPS time, the accuracy being around 1ms. If there is a GPS antenna available this is the most accurate method to perform synchronized measurements. The only limitation is that there must exist a clear line of sight between the GPS antenna and the sky in order for the transmited signal from the sattelites above earth to reach our receiver. The more part of the sky the antenna can see the better precision we are going to get, because GPS receivers use at least 4 sattelites to pinpoint their position accurately.

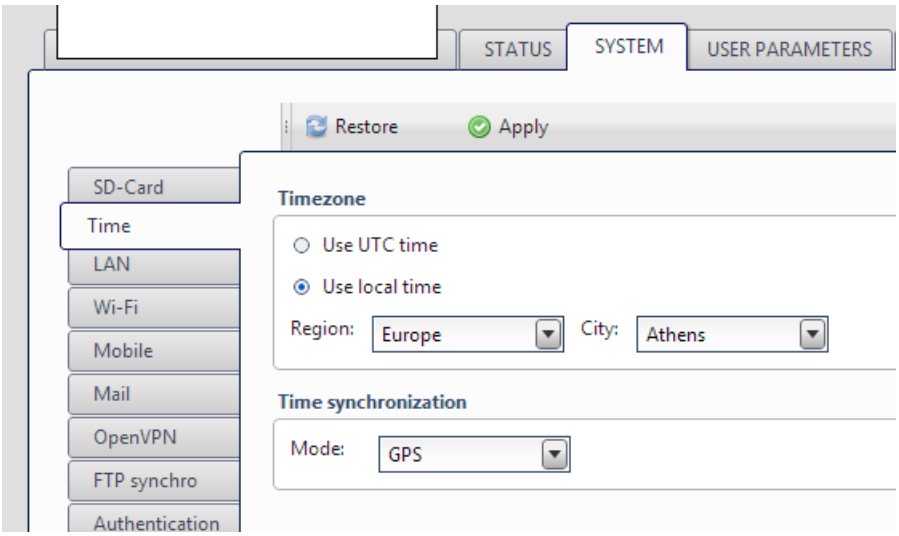

Figure 2.11: The System - Time tab

2.4.2 System - Lan

From this tab we can configure the properties of the MRs ethernet adapter. We can choose between DHCP (automatic) and Static IP Address assigning according to our setup, as described in the previous section (Section 2.3 - Connecting to the MR).

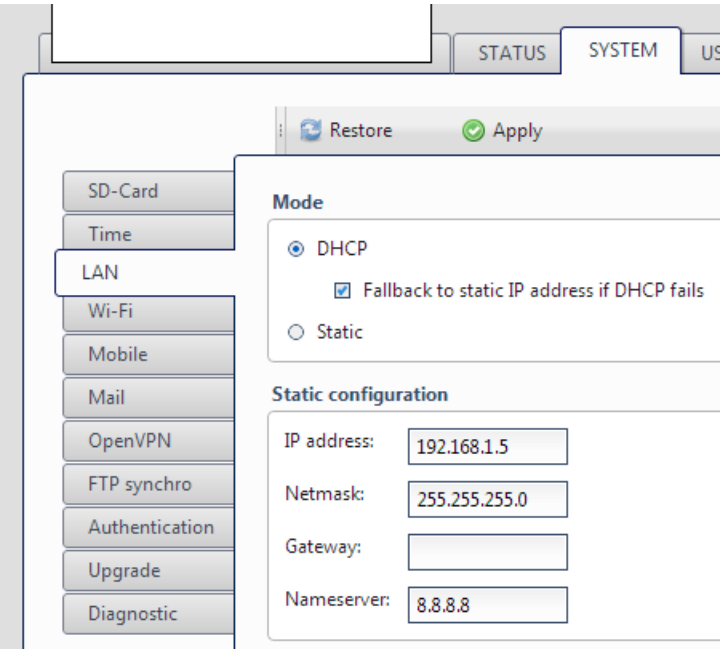

Figure 2.12: The System - LAN tab

2.4.3 Other tabs

The next important tabs are the *Acquisition, Trigger*, and *Record* tabs located in the *User Parameters* tab. In the *Acquisition* tab we set the sampling rate in Hertz. The sampling rate is the rate at which the MR takes samples from the continuous signal of the sensor. The highest sampling rate we can achieve is 1kHz.

In the *Trigger* tab we set the acceleration level (mg) which if surpassed the MR starts recording. This can be the acceleration in the X,Y, or Z axes or any combination of them. The trigger feature is mainly used in permanent sensor networks where we want to be warned if the vibration exceeds a certain level.

The *Record* tab is used to manualy trigger the recording process. We can either start recording by pressing the Start button, or we can specify a certain time as a starting point. There is also the possibility of performing repeated measurements at specific time intervals. This feature is of special interest to us because it applies to the one-day measurements that will be presented in the next chapter. The idle time between the measurements was designed to give us enough time to move the sensors from one position to the other. The reason of doing that along with the general design of the measurements is the topic of the third chapter.

Finally, we can easily download the measurement files to our computer from the *Event List* tab. We can choose between two file formats for the measurement files,

XMR and ASCII. XMR is a format that can be viewed by SYSCOM's free software EAWLight. This software is very simple and can only provide the plots of the time histories of the accelerations and their FFT(=Fast Fourier Transform). The ASCII format is a pure text file which has 3 columns, the accelerations in the X,Y, and Z axes in every sample. This format is convenient for analysis because it can be imported in numerical computation software such as MATLAB or Octave. After we have downloaded the measurement files, it is a matter of which software we are going to use for analysis. Each software requires the data to be imported in a specific format. Therefore, a in-between step is necessary in order to convert the measurements in the appropriate format.

2.4.4 Master-Slave configuration

The master-slave configuration is a very important feature of the measurement equipment. It applies only in the case of *wired* connection where all the MRs are in the same network. One specific MR is the Master,and the rest are the Slaves. The Master can force its own settings to the slaves. For example, we can set the time in the Master, and force the rest to be synchronized with it. This feature can be proved quite useful in cases where some of the instruments have to be placed in a closed and confined space where GPS signal is impossible. Using the Master-Slave configuration these instruments can be synchronized with the Master which can have it's own GPS (if we care about the real time) or a manual time (if we just want the measurements to be synchronized and do not care about the actual real time).

Another possibility offered by the Master-Slave configuration is *Common Triggering*. This feature is still experimental and will be implemented in future versions of the firmware. Common Triggering allows the simultaneous recording of all the instruments if at least one of them is triggered (manually of with trigger level).

2.5 The accelerometers

We should remind that even though all the configuration is done in the Motion Recorder, the actual measurement takes place in the accelerometer. It is the accelerometer that provides the Motion Recorder with the analog voltage signal which is then digitalized and processed. The accelerometer used is the MS2007+ Force Balance Accelerometer (5 triaxial and 3 uniaxial). It is capable of measuring frequencies in the range 0-80 Hz (80Hz is it's own natural frequency) which is a very good range for big structures like buildings or bridges. The MS2007+ is a highly sensitive instrument capable of measuring accelerations of just a few mg. It has a very large range of operating temperatures (-25° to 65° Celsius) and has a shock resistance of 30g. However the measuring range is up to 1g.

Force balance accelerometers are suitable for ambient vibration measurements because of their very high resolution in low frequency vibrations and because they can pick up microg accelerations. The basic principle of operation is Newtons Law. External motion is causing an internal mass to move inside the accelerometer. But this

movement is not allowed by an electrical feedback system which forces the mass to stay still by applying more electric current to a coil. The current developed in the coil is directly proportional to the force which is needed to keep the mass still, which in turn is proportional to the external acceleration through Newtons Second Law of motion. This type of accelerometer has a large inertial mass and is generally bigger than other types of accelerometers. This large mass results in large forces during high shock events and for this reason it is not suited to high shock environments.

Figure 2.13: The MS2007+ Force Balance Accelerometer

2.6 Connection Examples

In this section we present the 3 most fundamental setups that one might encounter in practice. Depending on the environment where the measurements are going to take place and on specific limitations of each situation, some features might be unavailable. For example, in a closed and confined space we might not be able to use GPS for time synchronization, or it might be physically impossible to have cables in specific parts of the structure. For these reasons one must be able to change the setup depending on the situation, and achieve good time synchronization and measurements as well. In the next figures we see the most common examples along with a description.

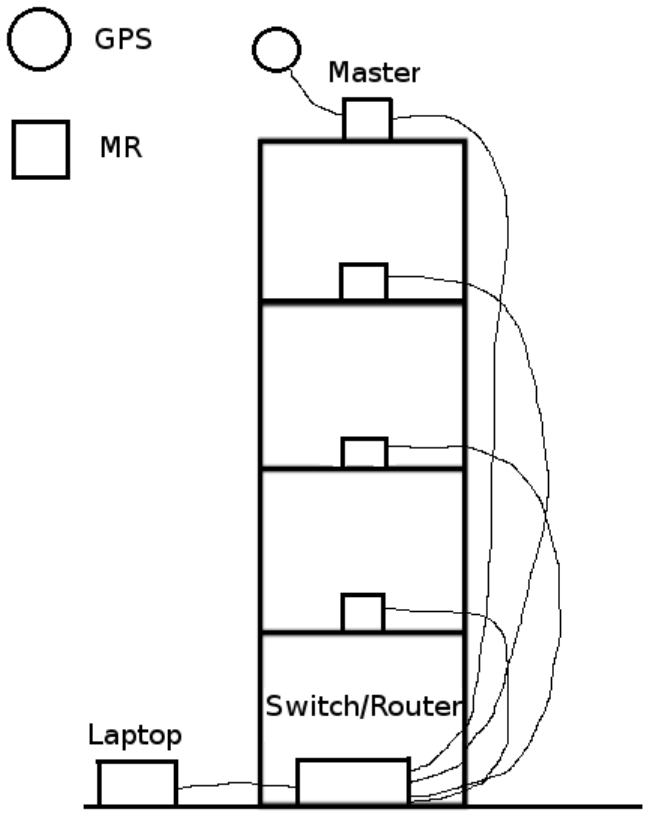

Figure 2.14: Connection setup 1

In this case, the recorders and the laptop are all connected with ethernet cables to the router/switch. Only the master recorder (serial number 22) has GPS connected to it and the rest synchronize with it. If not even the master can have GPS, then all recorders can still be synchronized with it, whether it gets the time manually or from an NTP server (if the router/switch has Internet access). The laptop can connect wired or wirelessly to the router and view all the recorders at the same time.

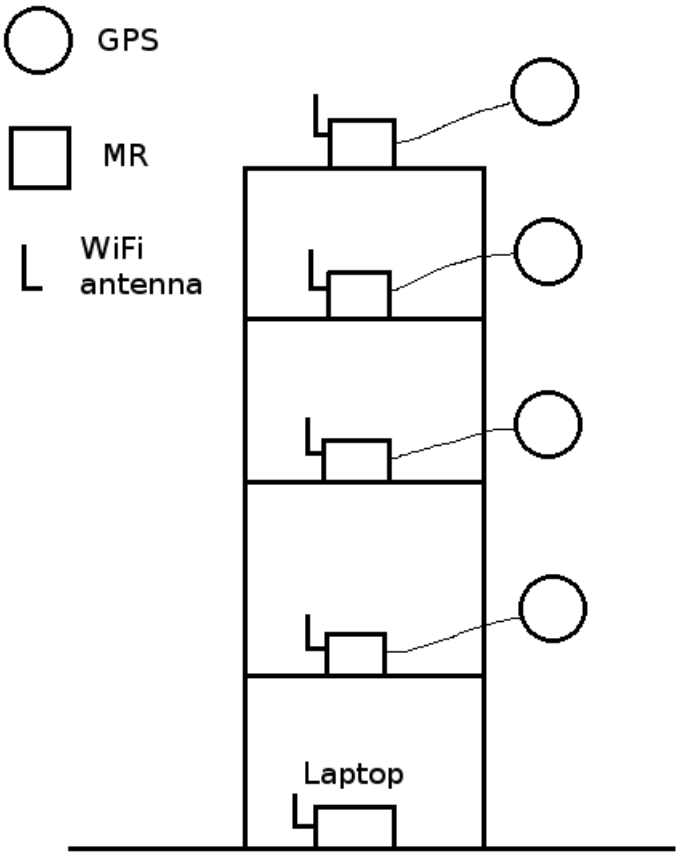

Figure 2.15: Connection setup 2

In this case we do not use any wires at all. Each recorder acts independently and has its own GPS. The laptop can view only *one* recorder each time by connecting wirelessly to the specific MR. Simultaneous configuration of all the recorders is not possible in this case. Also, for this method to work each GPS must have clear line of sight to the sky. The advantage compared to the previous method is that we do not need cables or a router/switch. That of course rules of the possibility of using PoE, and therefore every MR has to have its battery for power, or a AC/DC adapter if there is a power supply available.

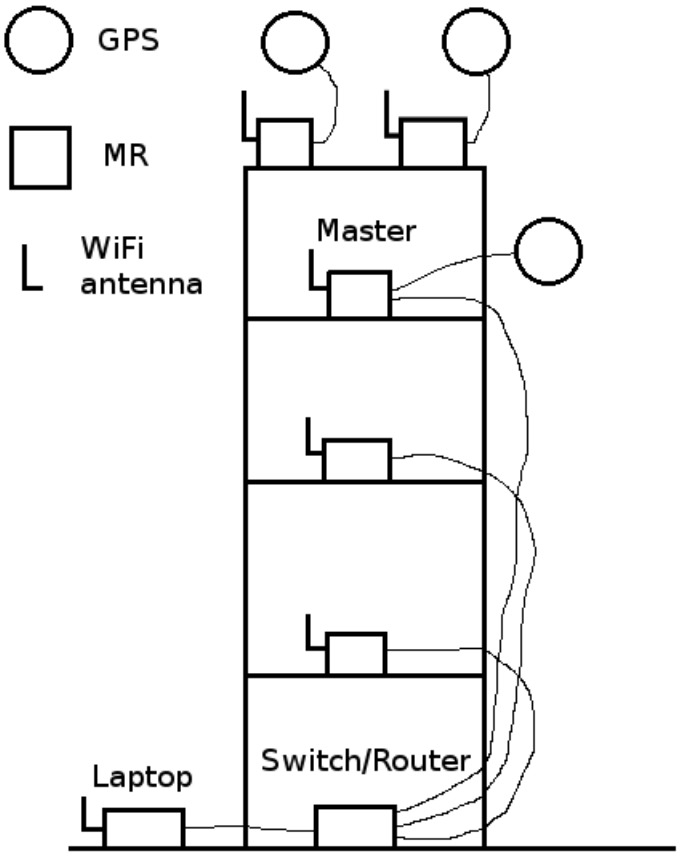

Figure 2.16: Connection setup 3

This case is a combination of the first 2 cases. It applies in the more realistic scenario where we have some limitations because of the structure itself. For example some instruments might not be able to have clear line of sight to the sky, or we might not be able to run cables from some recorders. Even if this is the case, we would still like to be able to perform synchronized measurements. In the figure shown above, we achieve that by synchronizing the inside recorders (no GPS) with one of the outside recorders (GPS), and using GPS for each of the rest outside recorders. The recorder that will synchronize the inside recorders must be the master. The control and configuration of the recorders is as described in the first two cases. The outside recorders are accessible by our laptop via wireless connection, one at a time. They have the correct real time because of the GPS. The inside recorders are accessible simultaneously from our laptop which must be connected to the same router/switch as shown in the picture. Each one can still be accessed wirelessly, but since they are in the same network it is more convenient to manage them from a computer that is in the network rather than independently. The fact that the master recorder (which

does have GPS) is connected in the same router enables it to share its real time with the inside recorders which can not have GPS. This can be the case if the master requires a long GPS cable in order to reach the outside and we only have one long cable.

After we have ensured that all the recorders have the same time, we can set a timed recording at a specific time and have a synchronized measurement from all our sensors. The features described above provide us with many different capabilities as far as our sensor network is concerned. Depending on the situation encountered each time, one may prefer one method over the other.

2.7 Convenience issues - Sensor Units

As we have already seen, the measurement system consists of the accelerometer, the Motion Recorder, its battery, the GPS, and their cables. When measuring vibrations in a large structure like a bridge, it is necessary to take measurements in many points of the structure, but the number of available sensors is usually much less than that. So we have to move our sensors from one place to another to cover these points. This process can consume a lot of time, if we have to carry all the separate devices independently, and can be potentially dangerous and inconvenient. For this reason all the individual devices required for a sensor to work (MR,battery,GPS,cables) were packed together in one sensor unit. In the following picture we can see the steel frame that was specifically constructed to hold all the parts together. This frame can be easily carried from one place to another as a single unit with safety. Only the accelerometer needs to be removed each time in order to place it where we want, whereas the WiFi antenna and the GPS stand outside of the frame in order to have clear signals. All of the cables remain connected and inside the frame during the movement of the unit so as to ensure continuous operation. This structure enables us to transfer the sensors easily in order to cover all the desired measurement points.

However, this also gives rise to two important issues. The first is the selection of the points that we are going to measure, and the second is how we are going to combine the measurements from different locations in the structure. These questions are the subject of chapters 5 and 6.

Chapter 3

Theoretical model of the Metsovo Bridge

In this chapter we are going to present the theoretical (FEM) model of the bridge. The theoretical model is useful in several ways, especially in determining the optimal sensor location as illustrated in Chapter 6.

3.1 Description of the Metsovo Bridge

The ravine bridge of Metsovo in section 3.2 (Anthohori-Anilio tunnel) of Egnatia Motorway is crossing the deep ravine of Metsovitikos river, 150m over the riverbed. This is the highest bridge of the Egnatia Motorway, with the height of the tallest pier equal to 110m. The total length of the bridge is 537m. The bridge has 4 spans of length 44.78m, 117.87m, 235m, 140m and 3 piers of which M1(45m) supports the boxbeam superstructure through pot bearings (movable in both horizontal directions), while M2(110m) and M3(35m) piers connect monolithicaly to the structure.

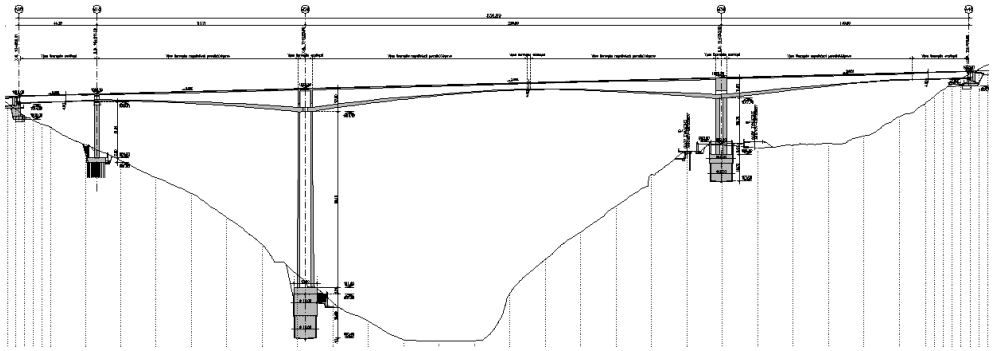

Figure 3.1: Longitudinal view of the Metsovo ravine bridge

Figure 3.2: The ravine bridge of Metsovo

Figure 3.3: The ravine bridge of Metsovo

The detailed geometry of the bridge is complicated because the piers have variable cross-sections and the deck is also inclined. A detailed design of the bridge can be found in V. Kelantonis (2010). In this work, one can find detailed instructions on how to design the 3D model of the Metsovo bridge in SolidWorks from the 2D drawings provided by Egnatia Odos. In the next figures we see the final 3D model.

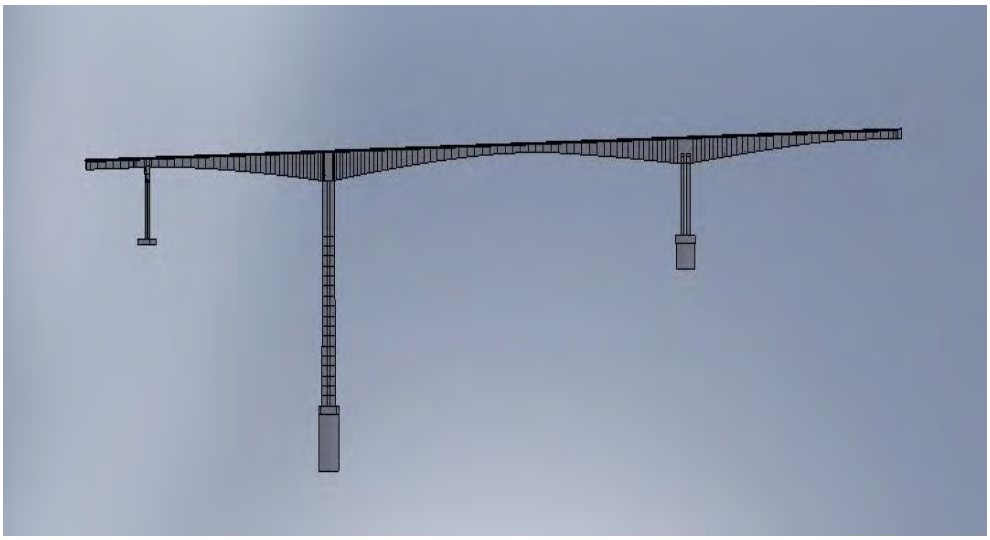

Figure 3.4: 3D model in SolidWorks

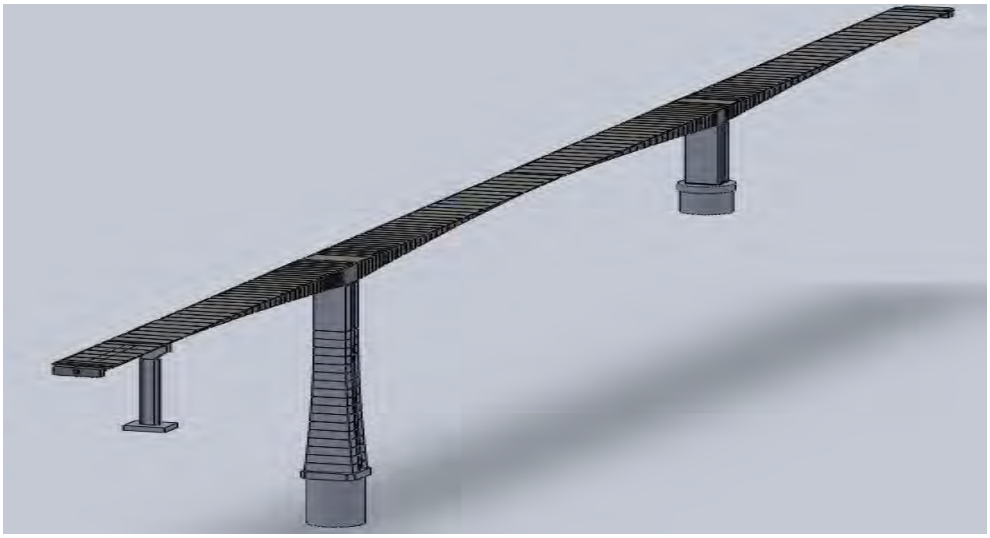

Figure 3.5: 3D model in SolidWorks

In this thesis we directly use the 3D SolidWorks model to import it into COMSOL Multiphysics for Finite Element Analysis. We are interested in eigenfrequency analysis. Specifically, we would like to obtain the modeshapes of the bridge as these are predicted by the Finite Element Method.

3.2 Finite Element Model of the Metsovo Bridge

The Finite Element model of the bridge was created by importing the 3D SolidWorks model into COMSOL. Then we specified the boundary conditions which are fixed bases of the piers and the rest of the structure is unconstrained and unloaded. The material of the bridge is reinforced concrete with density $2548 kg/m^3$ and modulus of elasticity 37GPa and 34GPa for the deck and the rest of the components respectively, according to the drawings by Egnatia Odos S.A. The model was meshed with extra coarse mesh and consists of 97.636 elements and 563.586 degrees of freedom.

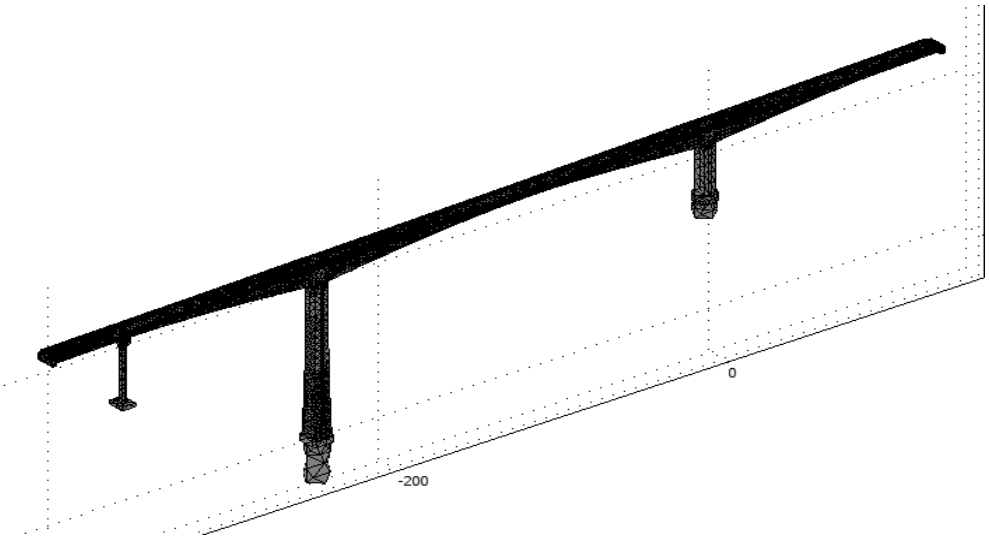

Figure 3.6: Finite Element model of the Metsovo Bridge

Eigenfrequency analysis was performed for the first 30 modes of the bridge. It is very important to have an accurate estimation of the mode shapes (and frequencies) before the actual measurements take place. That is because we would like to know the frequency bands we will be working on, but more important, the mode shapes can help us decide where on the structure to place our sensors and more specifically our *reference* sensors. It is important to know, at least roughly, in which points a specific mode shape has *nodes*, that is, points that have zero displacement in that mode. The reason is that our accelerometer in that specific point, will not be able to pick up any vibration of that specific mode. Therefore it is very important not to have reference sensors in nodes. In the next pages we present the 30 first modeshapes of the Metsovo bridge, as these are predicted by the Finite Element Method.

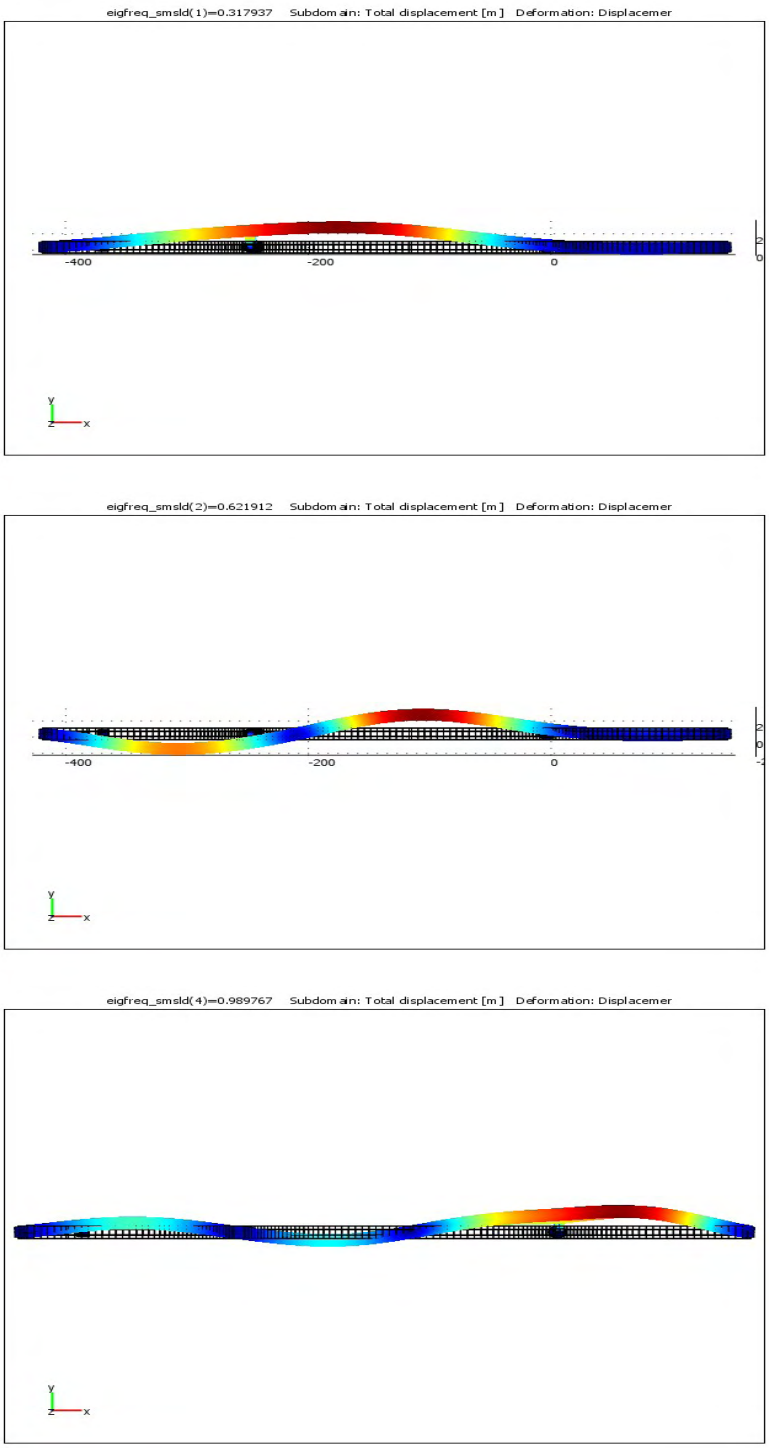

Figure 3.7: The 13 first transverse modes of Metsovo Bridge (1-3)

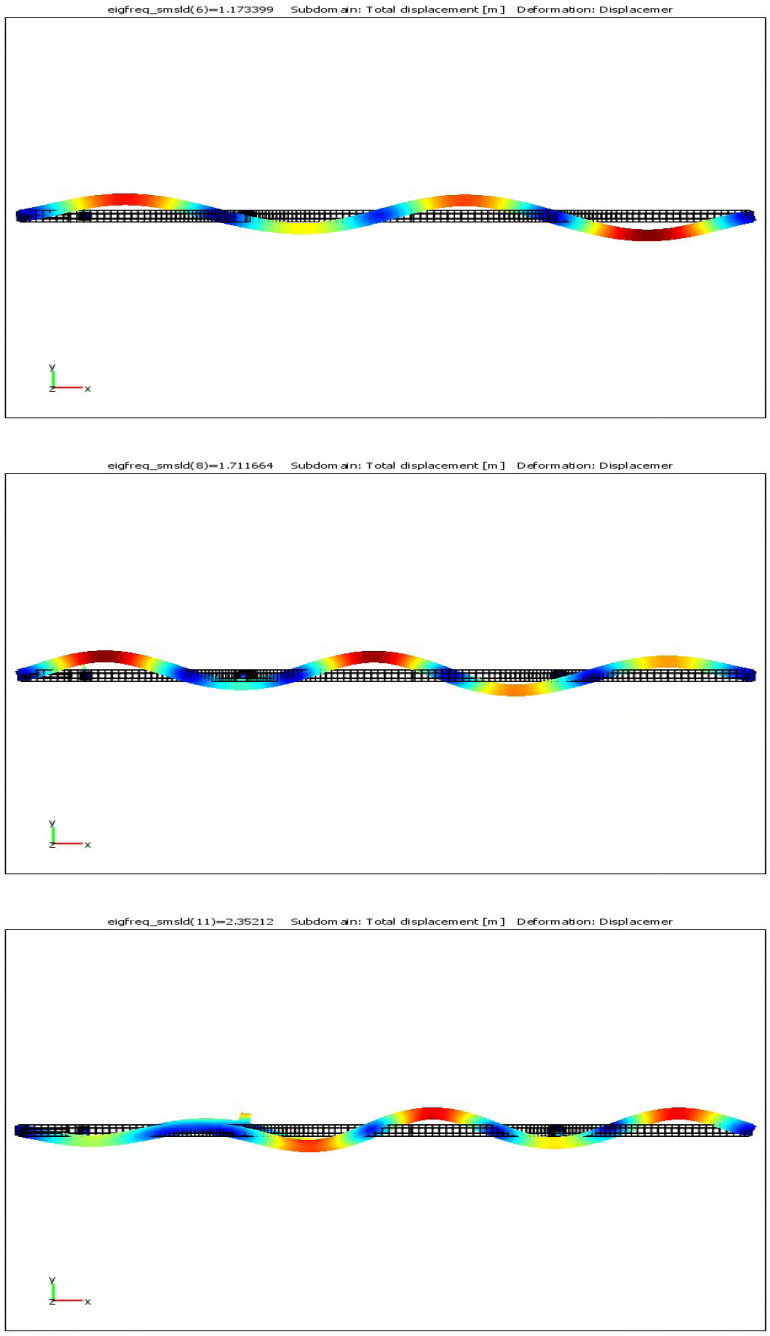

Figure 3.8: The 13 first transverse modes of Metsovo Bridge (4-6)

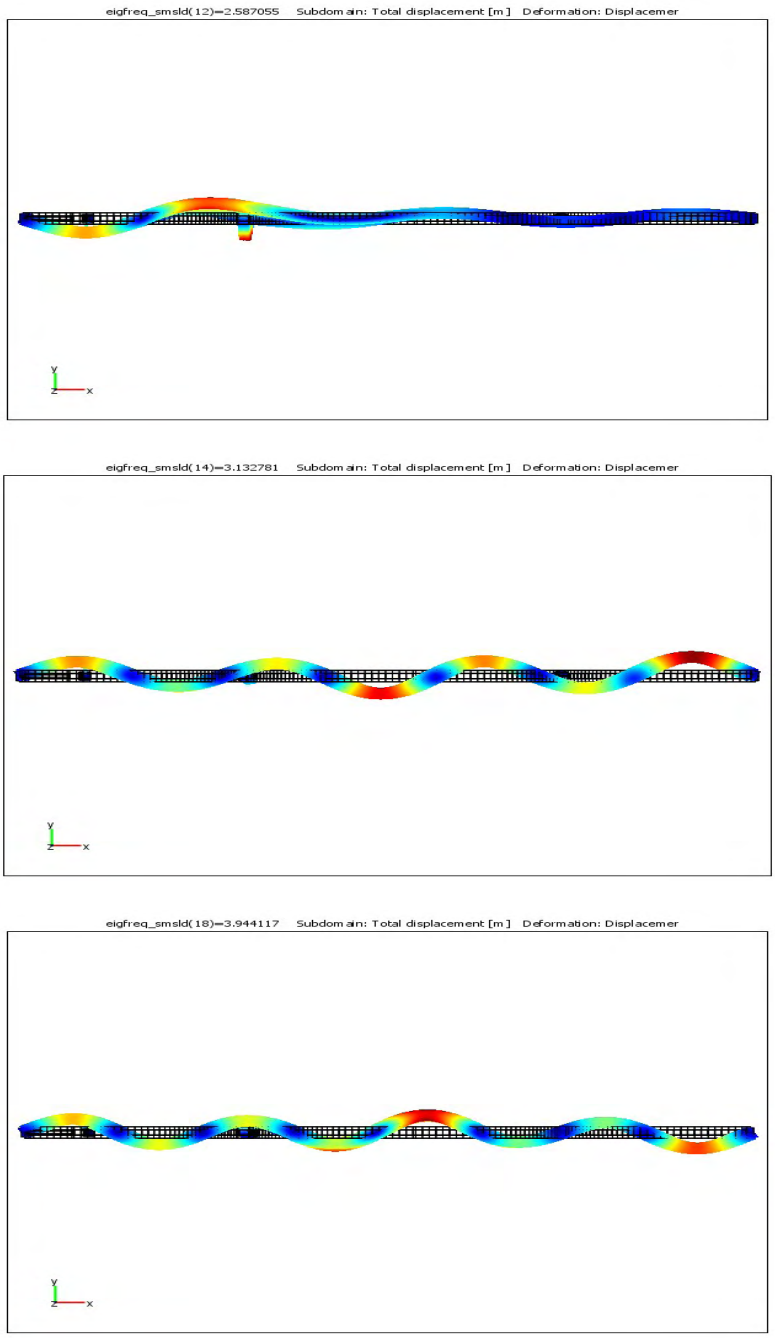

Figure 3.9: The 13 first transverse modes of Metsovo Bridge (7-9)

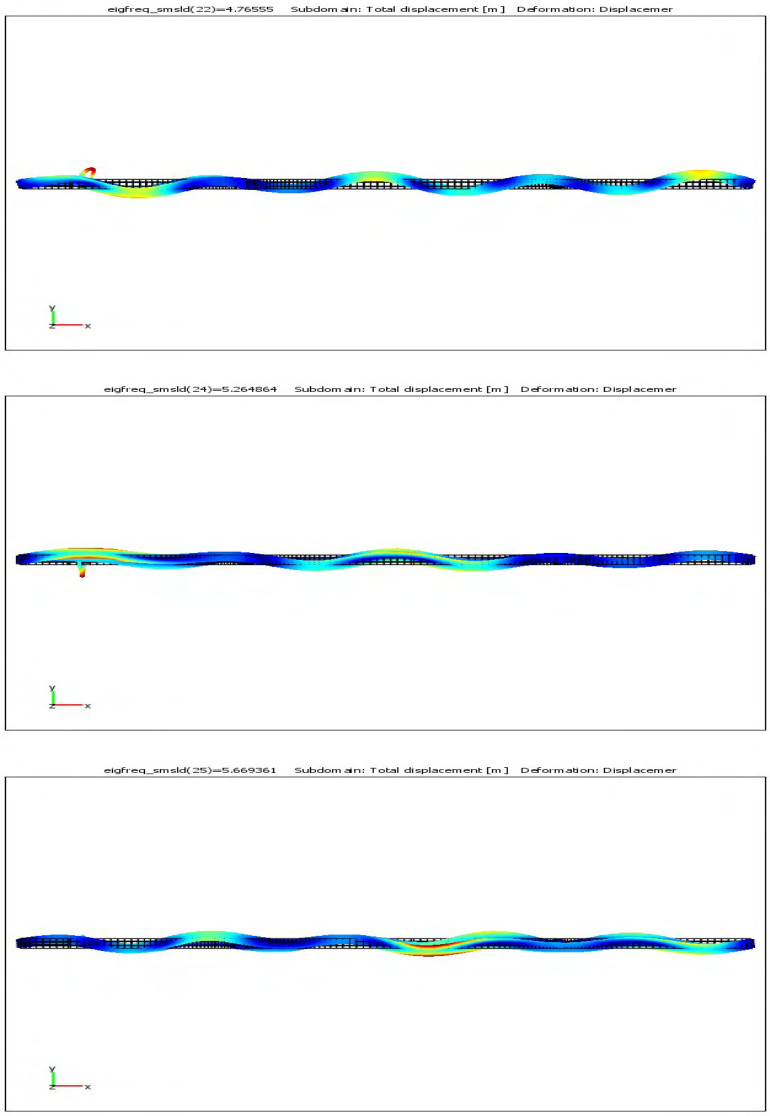

Figure 3.10: The 13 first transverse modes of Metsovo Bridge (10-12)

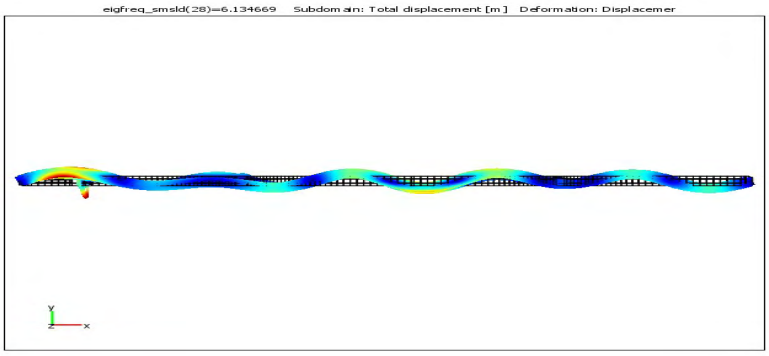

Figure 3.11: The 13 first transverse modes of Metsovo Bridge (13)

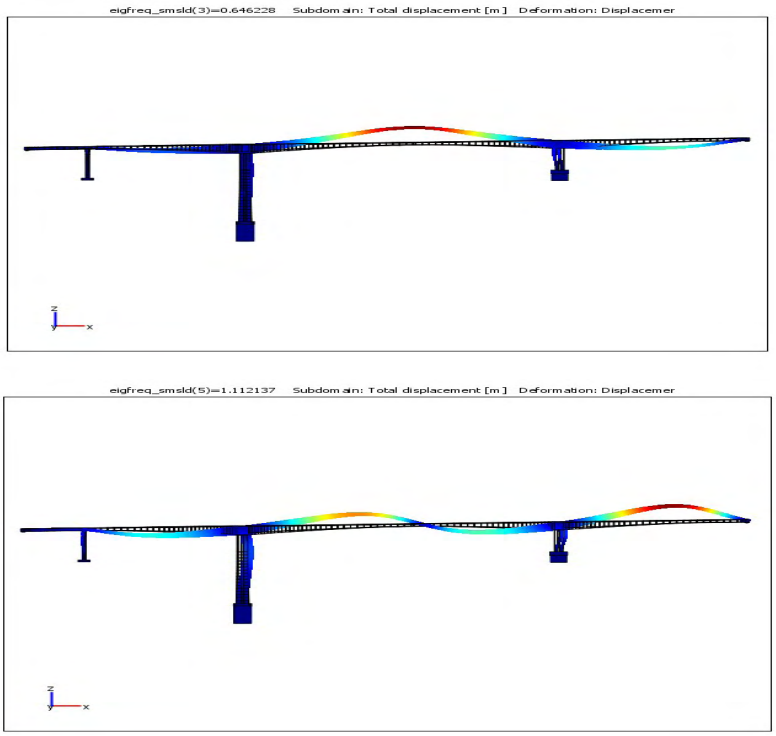

Figure 3.12: The 15 first bending modes of Metsovo Bridge (1-2)

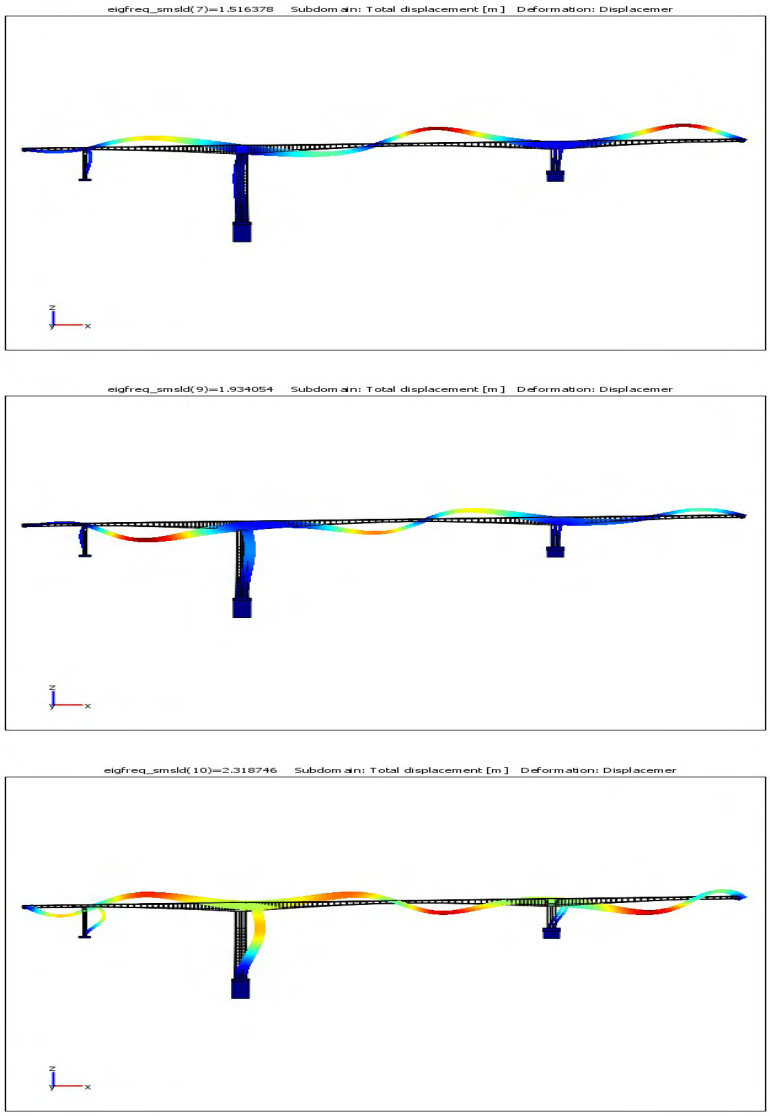

Figure 3.13: The 15 first bending modes of Metsovo Bridge (3-5)

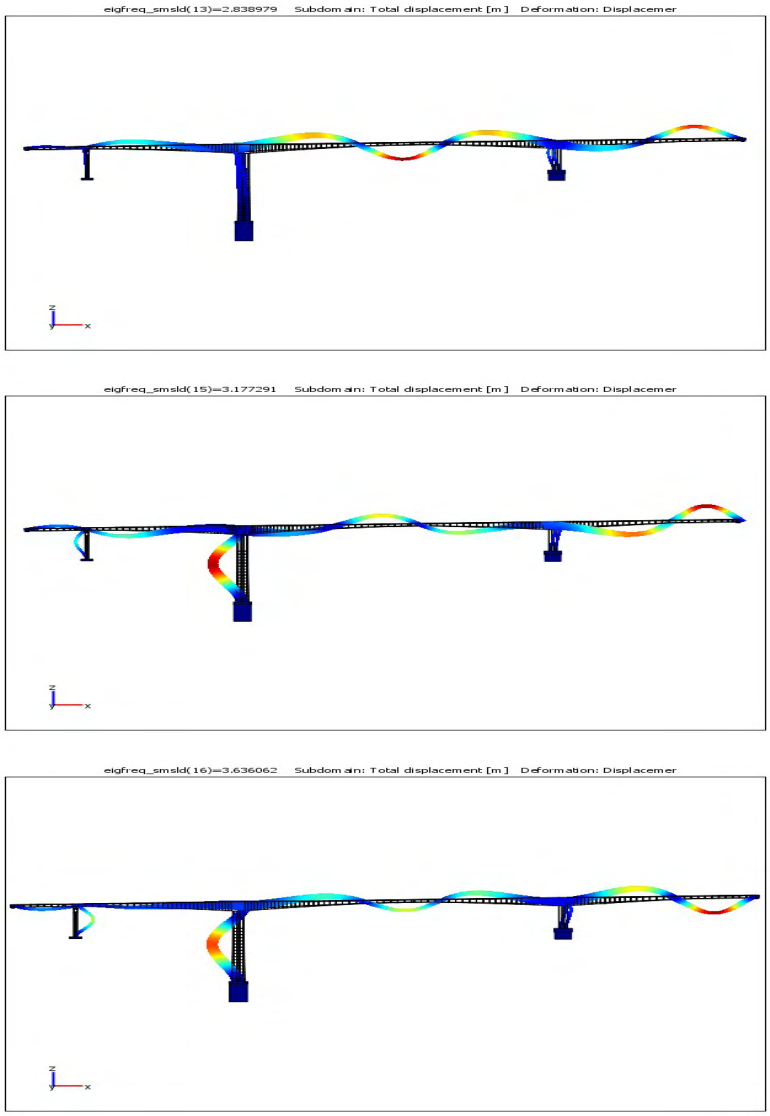

Figure 3.14: The 15 first bending modes of Metsovo Bridge (6-8)

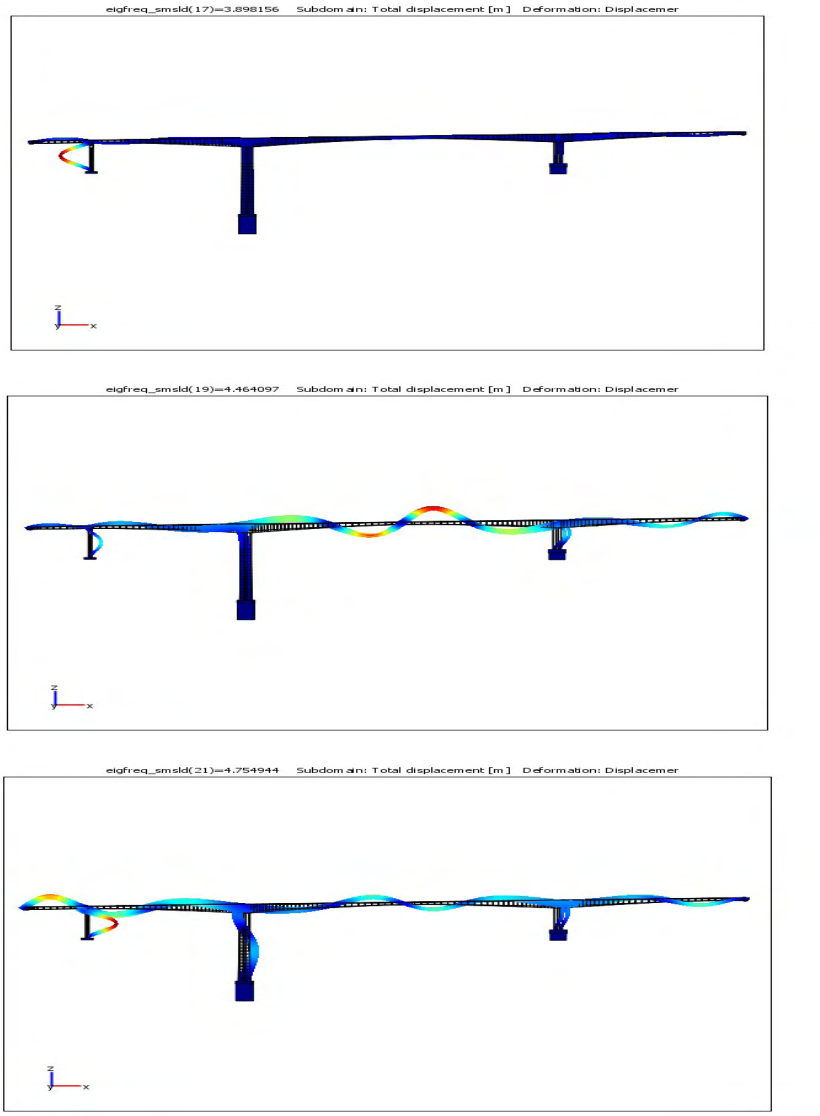

Figure 3.15: The 15 first bending modes of Metsovo Bridge (9-11)

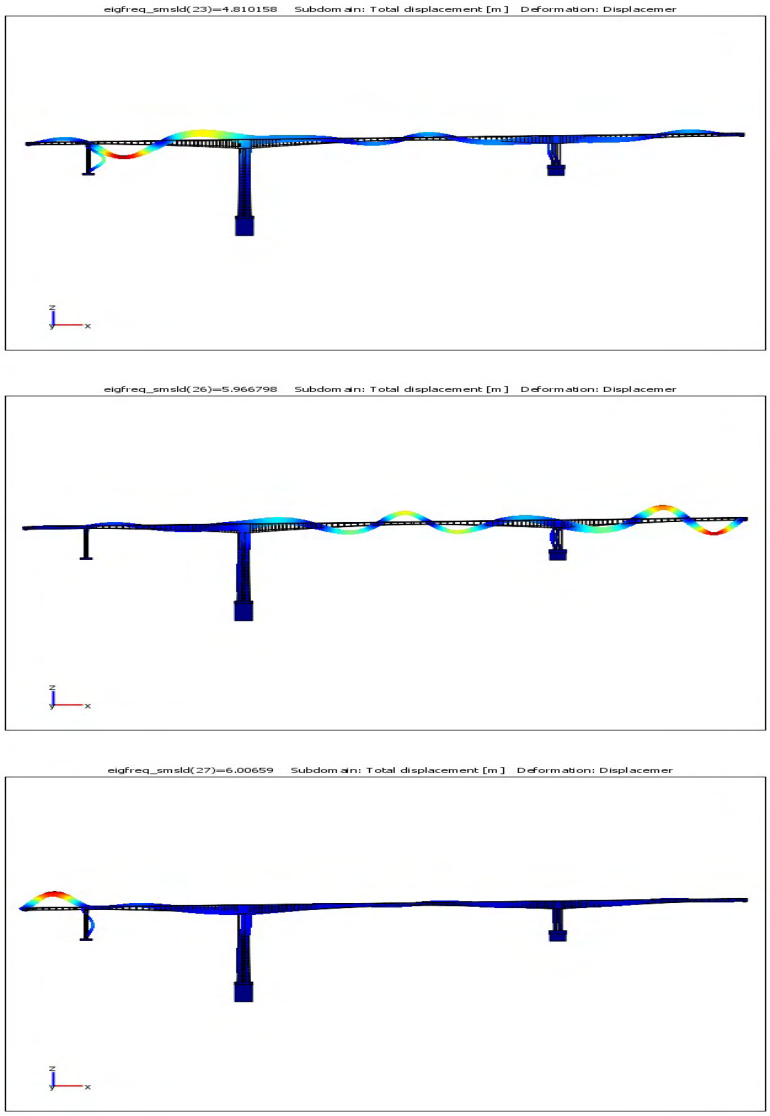

Figure 3.16: The 15 first bending modes of Metsovo Bridge (12-14)

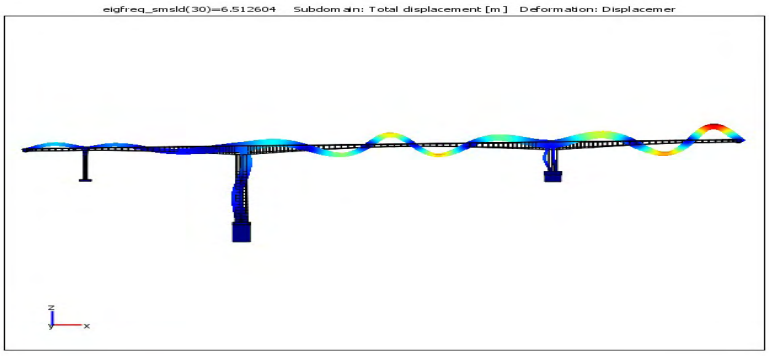

Figure 3.17: The 15 first bending modes of Metsovo Bridge (15)

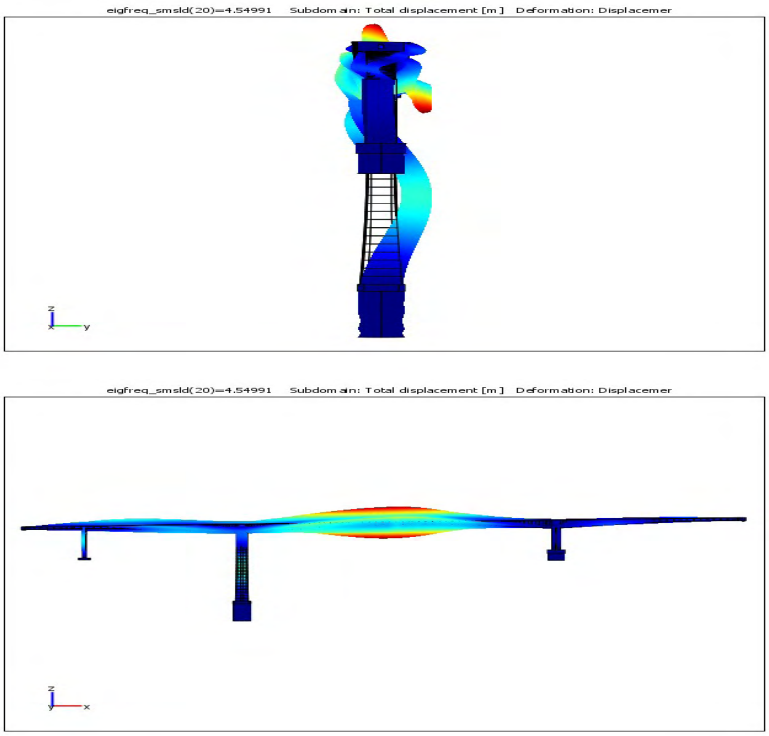

Figure 3.18: The 5 first torsional modes of Metsovo Bridge (1)

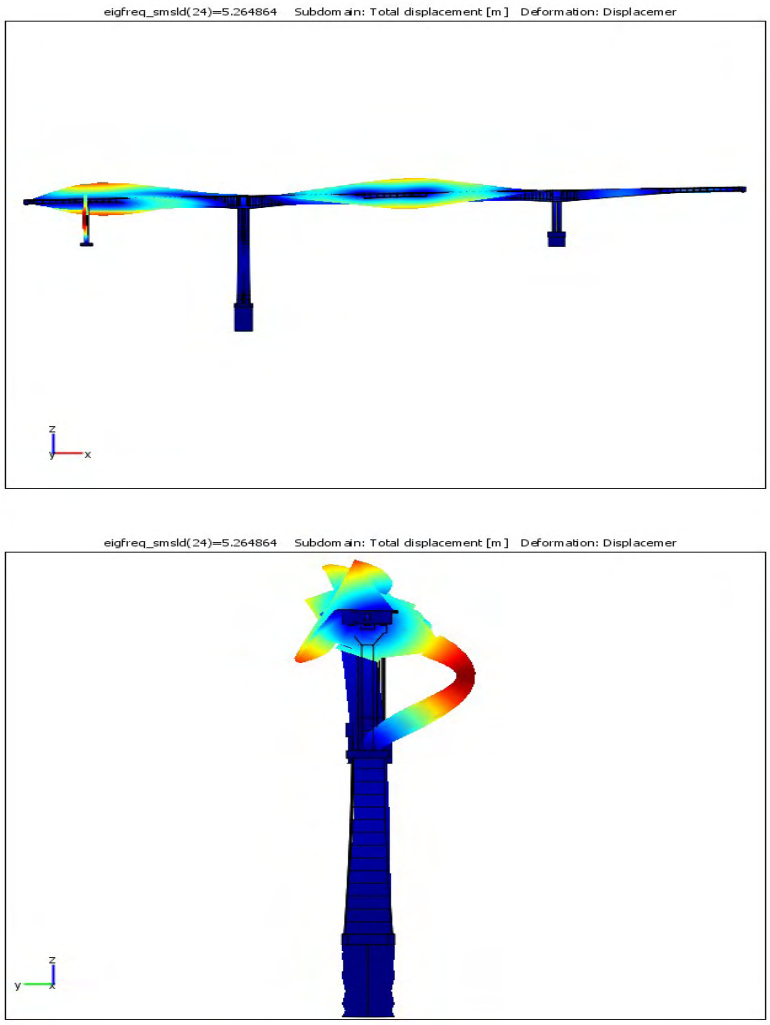

Figure 3.19: The 5 first torsional modes of Metsovo Bridge (2)

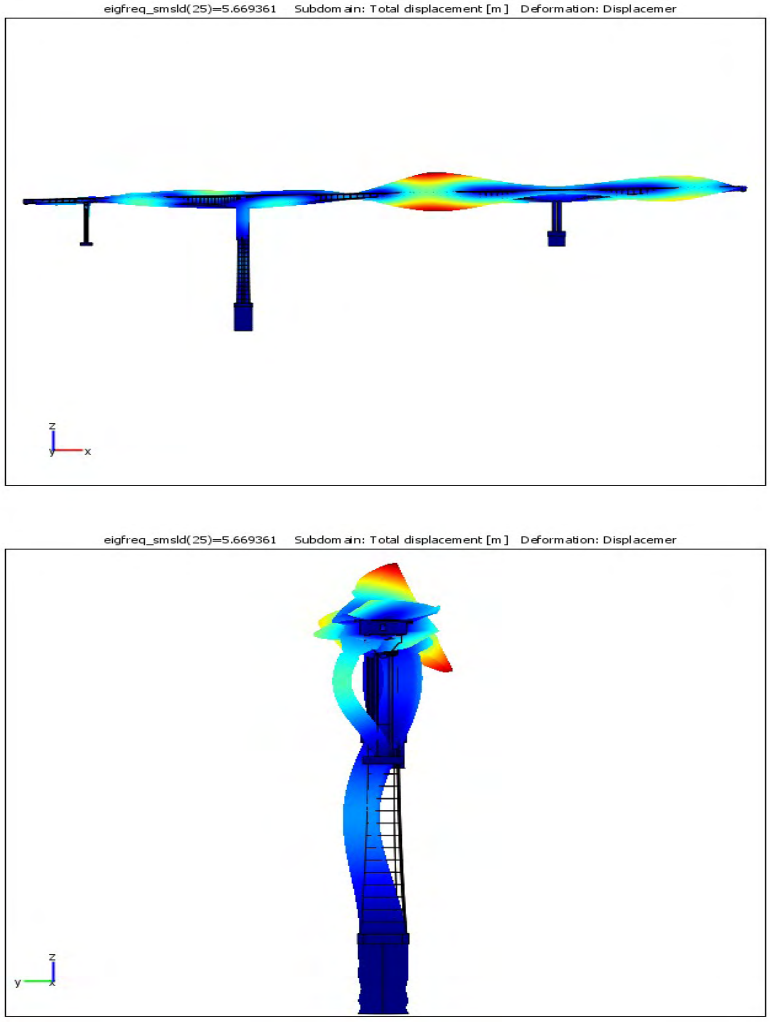

Figure 3.20: The 5 first torsional modes of Metsovo Bridge (3)

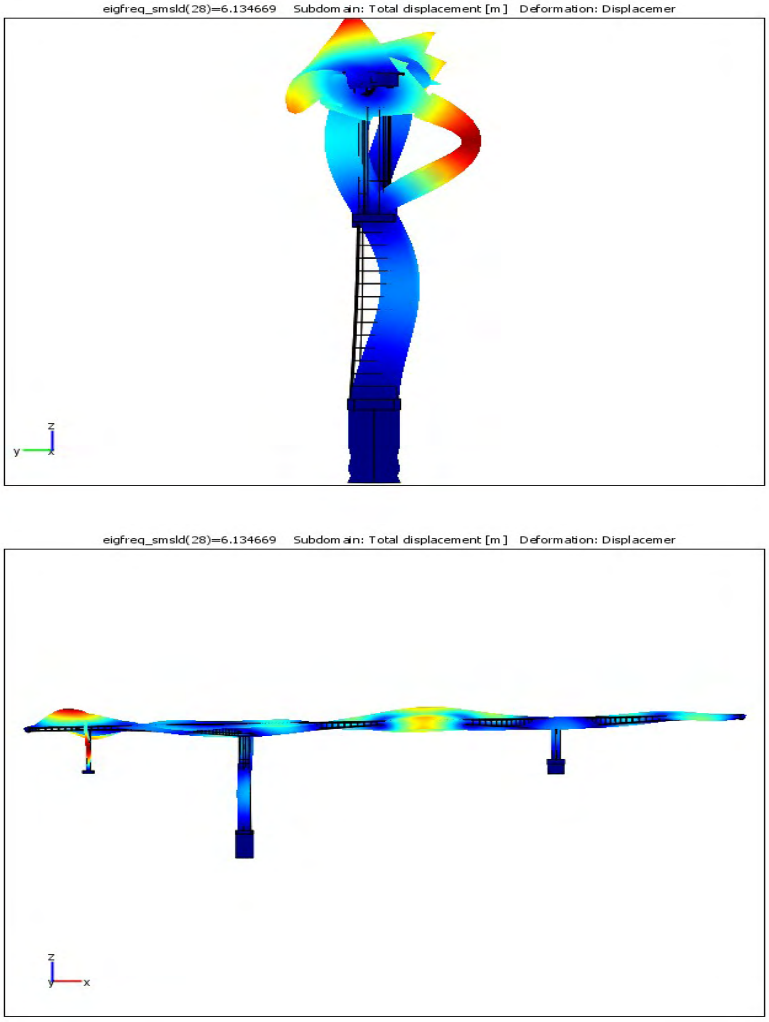

Figure 3.21: The 5 first torsional modes of Metsovo Bridge (4)

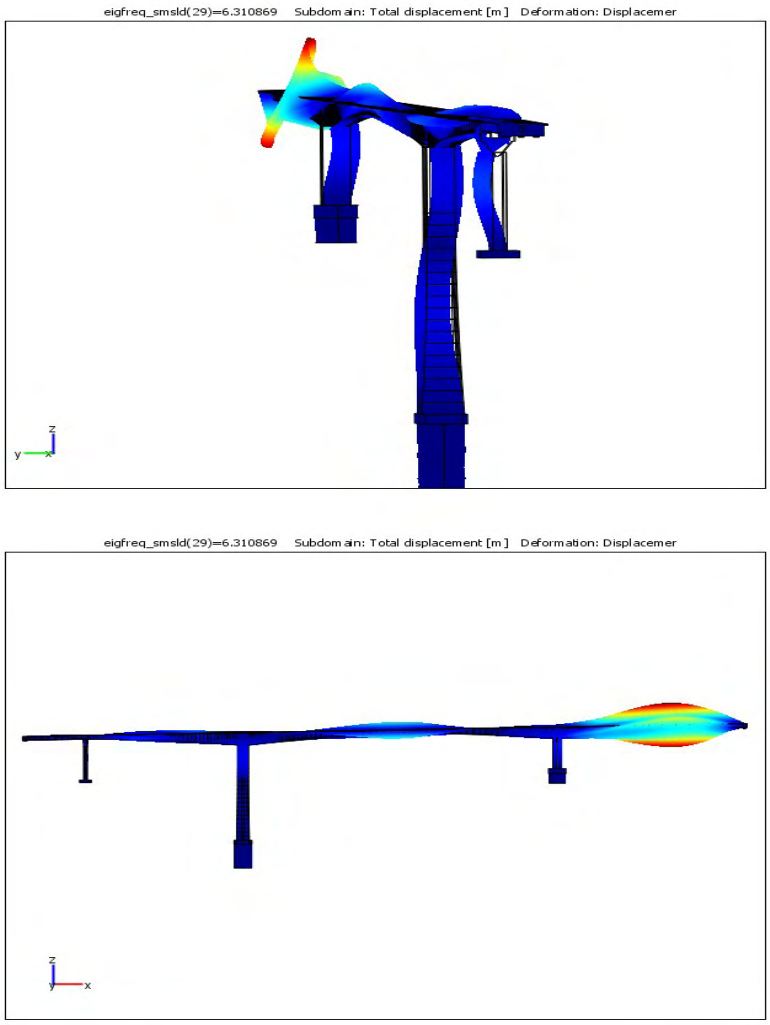

Figure 3.22: The 5 first torsional modes of Metsovo Bridge (5)

Note: Some modes are mixed (transverse and torsional) and appear in both lists.

Chapter 4

Modal Analysis

Generally there are two ways to perform modal analysis, depending on the source of the excitation. When the input is known we talk about input-output methods. In this case we apply a known input to the system and measure the output. When the input is unknown we talk about output-only methods. These methods involve measuring only the output of the structure in response to ambient excitation. Ambient excitations include loadings that may occur from wind, micro-earhquakes, vehicular and pedestrian traffic, and ocean waves. A basic assumption is that the ambient excitation is assumed to be a stationary random process containing a flat frequency spectrum.

Input-output methods have the advantage of suppressing noise effects on the structural response, which output-only methods do not have. However, input-output solutions tend to be more expensive than output-only solutions and usually create a disruption in the regular use of the structure. Output-only solutions allow for continuous uninterrupted structural health monitoring because the structural response can be measured under operating conditions (Operational Modal Analysis). Nonetheless, output-only methods have the disadvantage that excitation forces are unknown and are not always able to excite the higher frequency modes of the structure.

In the context of this thesis output-only measurements were used. Specifically, we used acceleration time histories from different points of the bridge. The analysis of the acceleration time histories in order to extract the modal properties was done with the MITooL software of the SDLab. In the next pages we present a brief overview of the theory of operational modal analysis.

4.1 Operational Modal Analysis

In this type of vibration, both excitation and response are described by random processes. Although it might be thought that this case could be treated in much the same way as experimental modal analysis (measured input excitation) this is not possible because the inherent properties of random signals cause them to violate the Dirichlet conditions. As a result, neither excitation nor response signals can be subjected to a valid Fourier Transform calculation and another approach must be used.

We introduce two sets of parameters which are used to describe *random* signals, one based in the time domain - the correlation functions - and the other in the frequency domain - the spectral densities [Lutes and Sarkani 2004]. We shall attempt here to provide some insight into these quantities without necessarily detailing all the background theory.

Consider a random signal $X(t)$, which will be assumed to be ergodic. The auto-correlation function is defined as the expected value of the product $X(t)X(t+\tau)$ computed along the time axis. This will always be a real and even function of time, and is written:

$$R_{XX}(\tau) = E[X(t)X(t+\tau)] \tag{4.1}$$

This correlation function, unlike the original quantity X(t), does satisfy the requirements for Fourier transformation and thus we can obtain its Fourier Transform by the usual equation. The resulting function we call a Spectral Density, in this case the Auto- or Power Spectral Density (PSD), $S_{XX}(\omega)$, which is defined as:

$$S_{XX}(\omega) = \frac{1}{2\pi}\int_{-\infty}^{\infty} R_{XX}(\tau)e^{-i\omega\tau}\,d\tau \tag{4.2}$$

The Power Spectral Density is a real and even function of frequency, and does in fact provide a description of the frequency composition of the original function, X(t).

A similar concept can be applied to a pair of functions such as f(t) and x(t) to produce *cross correlation* and *cross spectral density* functions. The cross correlation function, $R_{xf}(\tau)$, is defined as:

$$R_{xf}(\tau) = E[x(t)f(t+\tau)] \tag{4.3}$$

and the cross spectral density (CSD) is defined as its Fourier Transform:

$$S_{xf}(\omega) = \frac{1}{2\pi}\int_{-\infty}^{\infty} R_{xf}(\tau)e^{-i\omega\tau}\,d\tau \tag{4.4}$$

Cross correlation functions are real, but not always even, functions of time, and cross spectral densities, unlike auto spectral densities, are generally complex functions of frequency with the particular conjugate property that:

$$S_{xf}(\omega) = S^*_{fx}(\omega) \tag{4.5}$$

Now that we have established the necessary parameters to describe random processes in general, we are in a position to define the input/output relationships for systems undergoing random vibration [Ewins 2000]. In deriving the final equations which permit the calculation of response from known excitations, we shall not present a full analysis; rather, we shall indicate the main path followed without detailing all the algebra. In this way, we hope to demonstrate the basis of the analysis and the origins of the final expressions, which are the only ones required in normal modal testing practice.

The analysis is based on the general excitation/response relationship in the time domain, also known as *Duhamel's Integral*:

$$x(t) = \int_{-\infty}^{\infty} h(t-t')f(t')\,dt' \tag{4.6}$$

Using this property, it is possible to derive an expression for $x(t)$ and another for $x(t+\tau)$ and thus to calculate the response autocorrelation function $R_{xx}(\tau)$:

$$R_{xx}(\tau) = E[x(t)x(t+\tau)] \tag{4.7}$$

This equation can be manipulated to describe the response autocorrelation in terms of the corresponding property of the excitation, $R_{ff}(\tau)$, but the result is a complicated and unusable triple integral. However, this same equation can be transformed to the frequency domain to emerge with the very simple form:

$$S_{xx}(\omega) = |H(\omega)|^2 S_{ff}(\omega) \tag{4.8}$$

Although apparently convenient, equation (4.8) does not provide a complete description of the random vibration conditions. Further, it is clear that it could not be used to determine the FRF (Frequency Response Function) from measurements of excitation and response because it contains only the modulus of $H(\omega)$, the phase information being omitted from this formula. A second equation is required and this may be obtained by a similar analysis based on the cross correlation between the excitation and the response, the frequency domain form of which is:

$$S_{fx}(\omega) = H(\omega)S_{ff}(\omega) \tag{4.9}$$

or, alternatively:

$$S_{xx}(\omega) = H(\omega)S_{xf}(\omega) \tag{4.10}$$

So far, all the analysis in this section has been confined to the case of a single excitation parameter, although it is clear that several responses can be considered by repeated application of the equations (4.8) and (4.10). In fact, the analysis can be extended to situations where several excitations are applied simultaneously, whether or not these

are correlated with each other. This analysis involves not only the autospectra of all the individual excitations, but also the cross spectra which link one with the others. The general input/output equation for this case is:

$$[S_{fx}(\omega)] = [S_{ff}(\omega)][H(\omega)] \tag{4.11}$$

The pair of equations (4.8) and (4.10) provides us with the basis for a method of determining a system's FRF properties from the measurement and analysis of a random vibration test. Using either of them, we have a simple formula for determining the FRF from estimates of the relevant spectral densities:

$$H(\omega) = \frac{S_{fx}(\omega)}{S_{ff}(\omega)} \tag{4.12}$$

or

$$H(\omega) = \frac{S_{xx}(\omega)}{S_{xf}(\omega)} \tag{4.13}$$

As far as the excitation is concerned, in operational modal analysis we assume that the excitation is a *white noise process* containing a *constant frequency spectrum*. There must not be harmonic excitations present because they will appear as peaks in the otherwise flat spectrum of the excitation, and this will also cause the response to have peaks in the frequencies of the harmonic excitations which will not be modal frequencies.

At this point we shall remind that the very estimation of the spectral density functions from the real measured signals includes the use of specific algorithms for that purpose. The MITooL software can be configured to use either of two available algorithms for spectral density estimation, namely a correlogram and periodogram approach. Therefore, the accuracy of the results depends on the accuracy of the estimation of the spectral densities from the measured signals. Several parameters of the algorithms can be changed for better results depending on the measured signal. A detailed analysis of the algorithms used in the MITooL software can be found in Ntotsios (2009).

After having estimated the CPSDs from real data, the next step is to compare them with the CPSDs predicted by the modal model of the structure, in order to obtain the modal properties which is our primary interest. The foundation of this comparison, lies in the fact that each FRF, $H(j\omega)$, can be written in the general form:

$$H(j\omega) = \sum_{r=1}^{N} \frac{\mathbf{u_r}\mathbf{l_r^T}}{j\omega - \lambda_r} + \frac{\mathbf{u_r^*}\mathbf{l_r^{*T}}}{j\omega - \lambda_r^*} \tag{4.14}$$

where λ_r is the eigenvalue of the r^{th} mode (containing the eigenfrequency and damping ratio), $\mathbf{u_r}$ is the modeshape of mode r, and $\mathbf{l_r}$ is the participation factor of mode r.

Equation (4.14) forms the foundation of output-only modal analysis: it shows a direct connection between the modal properties of a system and its response characteristics. It is known from literature [Ljung 1999] that for stationary stochastic processes the cross power spectral density matrix $S_{xx}(j\omega)$ of the response vector $x(t)$ can be written as a function of the transfer function $H(j\omega)$ and the cross power spectral density matrix $S_{ff}(j\omega)$ of the unknown force vector $f(t)$ as follows:

$$S_{xx}(j\omega) = H(j\omega)S_{ff}(j\omega)H^{*T}(j\omega) \tag{4.15}$$

Assuming that the forces acting on the structure are white noise sequences, then the cross power spetral density matrix of the forces is constant, independent of $j\omega$, given by $S_{ff}(j\omega) = S_0$ that is real. In this case the above equation is written in the form:

$$S_{xx}(j\omega) = H(j\omega)S_0H^{*T}(j\omega) \tag{4.16}$$

It can be shown that by assuming white noise inputs and substituting equation (4.14) in the above equation the cross power spectral density matrix $S_{xx}(j\omega)$ of the responses evaluated at frequency ω, can be *modally* decomposed as follows:

$$S_{xx}(j\omega) = \sum_{r=1}^{N} \frac{\mathbf{u_r}\mathbf{g_r^T}}{j\omega - \lambda_r} + \frac{\mathbf{u_r^*}\mathbf{g_r^{*T}}}{j\omega - \lambda_r^*} + \frac{\mathbf{g_r}\mathbf{u_r^T}}{-j\omega - \lambda_r} + \frac{\mathbf{g_r^*}\mathbf{u_r^{*T}}}{-j\omega - \lambda_r^*} \tag{4.17}$$

where $\mathbf{u_r}$ is the complex modeshape of mode r and $\mathbf{g_r}$ is the operational reference vector for mode r. This reference vector is a complex function of the cross power spectrum matrix of the unknown random input forces and the modal parameters of the structure but its physical interpretation is less obvious than the modal participation factors. A detailed analysis of the derivation of equation (4.17) can be found in Ntotsios (2009). It should be noticed that the modal decomposition of the power densities of the outputs has a symmetry in the poles, i.e. both the positive and negative poles are present in the model. This symmetry is referred to as a 4-quadrant symmetry. Given this similarity between the modal decomposition of the cross spectral densities of the outputs and the modal decomposition of the FRFs, the modal parameter estimation techniques developed for FRFs can be extended to handle the case where the cross power spectral density matrix is available from output-only data.

The usual procedure - and the one followed by the MITooL software - is to use a curve-fitting algorithm. More specifically, a minimization is performed in order to fit the estimated CPSD matrix to the CPSD matrix predicted by the modal model, as in equation (4.17), with respect to the modal properties (natural frequencies, modeshapes, and associated damping ratios). The values of the modal properties that minimize the measure of fit between the predicted and experimental CPSDs are our best estimates. It is useful to remind that in order to use equation (4.17) for the identification of modal parameters from output-only data, accurate estimates of the cross power spectral densities between the responses, are to be obtained from finite sequences of measured time samples. The accuracy of the identified modal parameters depends highly on the accuracy of the estimation of the CPSDs.

Chapter 5

Mode Shape Assembly

5.1 Problem description

When modal analysis is performed on an estimated CPSD matrix of the measured responses we can extract certain modal properties for the r^{th} mode:

$$S_{xx}(j\omega) \rightarrow \omega_r,\, \zeta_r,\, \phi_{kr} : \, r = 1 \dots m,\, k = 1 \dots n \tag{5.1}$$

where m is the total number of identified modes and n is the total number of DOFs where we placed our sensors. Notice that we extract the modeshape matrix row elements ϕ_{kr} in the *specific* DOFs where the measurements were performed, namely the k^{th} row of the modeshape matrix for $k = 1 \dots n$. In order to obtain an accurate view of the mode shapes we need to extract the modeshape components in several DOFs, depending on the complexity of each mode. Higher modes tend to have more complex geometric shapes, and therefore require us to extract more modeshape components (increase the spatial resolution of modeshapes) in order to avoid the problem of spatial-aliasing.

However, in practical situations, there is only a limited number of available sensors and many points in the structure that need to be measured. This is the case in ambient vibration testing of large structures such as bridges or buildings. Obviously, it is impossible to measure all the desired DOFs at the same time, so we measure only a few of them at a time. The problem is the following:

Mode shapes identified from individual setups can have different sense and scaling. Depending on the number of reference DOFs (common DOFs among different setups) and the quality of identified mode shapes, implementation issues can arise when determining the optimal mode shape that compromise among different setups. In this chapter we are going to present a method for determining the optimal mode shape that fits the mode shapes identified from multiple setups in a least square sense. The method presented in this study, is a simplification of the method proposed by S.K. Au (2011) and uses the same symbols and notation. The measure of fit function is defined as the squared difference between the theoretical and identified mode shapes

suitably oriented and scaled to the same norm. The most important element of the method is the presence of *reference DOFs*. Since the mode shapes identified from individual setups are arbitrary in sense and scaling, common reference DOFs must be present across different setups in order to allow their mode shapes to be assembled. The reference DOFs must have significant frequency response in the modes of interest. There must also be at least one common reference DOF across any two setups.

5.2 Proposed methodology

Let n_s be the number of different setups, n_i be the number of measured DOFs in the i^{th} setup, and n be the total number of DOFs measured (in all setups). Let $\boldsymbol{\phi} \in R^n$ be the mode shape (for the r mode) covering the measured DOFs in all setups (unknown). Also, let $\hat{\boldsymbol{\phi}}_i \in R^{n_i}$ be the measured modeshape vector from the i^{th} configuration. Vector $\hat{\boldsymbol{\phi}}_i$ has n_i components because the i^{th} configuration had n_i DOFs measured. Note that $\sum_{i=1}^{n_s} n_i > n$ because some DOFs are measured in more than one configuration.

We need a way to compare the measured modeshape of the i^{th} configuration with the corresponding DOFs of the full unknown modeshape $\boldsymbol{\phi}$. This is achieved by using a selection matrix $\boldsymbol{L}_i \in R^{n_i \times n}$ defined for every configuration as : $\boldsymbol{L}_i(j,k) = 1$, if the j^{th} data channel in the i^{th} setup gives the k^{th} DOF of the full mode shape; and zero otherwise. Therefore, the mode shape $\boldsymbol{\phi}_i$ in the i^{th} setup can be mathematically related to the assembled mode shape $\boldsymbol{\phi}$ by:

$$\boldsymbol{\phi}_i = \boldsymbol{L}_i \boldsymbol{\phi} \quad , \quad \boldsymbol{\phi}_i \in R^{n_i} \tag{5.2}$$

Our objective is to determine the 'best' assembled mode shape $\boldsymbol{\phi}$ so that $\{\boldsymbol{\phi}_i : i = 1, \ldots, n_s\}$ are closest to their measured counterparts $\left\{\hat{\boldsymbol{\phi}}_i : i = 1, \ldots, n_s\right\}$ in a least square sense.

The optimal mode shape is formulated as the one that minimizes a measure-of-fit objective function. When formulating the objective function, the issue of scaling should be addressed. Each $\hat{\boldsymbol{\phi}}_i$ might be differently scaled, but the shapes of two vectors can only be compared fairly if they have the same Euclidean norm. This suggests that the discrepancy should be measured based on the difference between $\boldsymbol{\phi}_i$ and $c_i\hat{\boldsymbol{\phi}}_i$ rather than directly between $\boldsymbol{\phi}_i$ and $\hat{\boldsymbol{\phi}}_i$; in the former case both vectors have the same norm. The objective function that should be minimized is :

$$J(\boldsymbol{\phi}) = \sum_{i=1}^{n_s} \|\boldsymbol{\phi}_i - c_i\hat{\boldsymbol{\phi}}_i\|^2 \tag{5.3}$$

subject to the constraint:

$$\|\boldsymbol{\phi}\|^2 = 1 \Rightarrow \boldsymbol{\phi}^T\boldsymbol{\phi} = 1 \Rightarrow \boldsymbol{\phi}^T\boldsymbol{\phi} - 1 = 0 \tag{5.4}$$

Constrained optimization is converted to unconstrained using Lagrange multipliers as follows :

$$J(\boldsymbol{\phi}, \lambda) = J(\boldsymbol{\phi}) + \lambda(1 - \boldsymbol{\phi}^T\boldsymbol{\phi}) \tag{5.5}$$

In order to proceed we need to find the values of $c_i : i = 1, \ldots, n_s$

Optimal scaling factors

This is the part which significantly deviates from the methodology proposed by S.K. Au (2011), leading to a different form of the solution. In order to find the optimal c_i we now consider a different minimization problem with respect to c_i this time. Minimize the objective function :

$$G(c_i) = \|\boldsymbol{\phi}_i - c_i\hat{\boldsymbol{\phi}}_i\|^2 = (\boldsymbol{\phi}_i - c_i\hat{\boldsymbol{\phi}}_i)^T(\boldsymbol{\phi}_i - c_i\hat{\boldsymbol{\phi}}_i) \tag{5.6}$$

This minimization can be performed analytically as follows:

$$\begin{aligned}
\frac{\partial G}{\partial c_i} = 0 \Rightarrow -\hat{\boldsymbol{\phi}}_i^{\,T}(\boldsymbol{\phi}_i - c_i\hat{\boldsymbol{\phi}}_i) + (\boldsymbol{\phi}_i - c_i\hat{\boldsymbol{\phi}}_i)^T(-\hat{\boldsymbol{\phi}}_i) = 0 \\
\Rightarrow -\hat{\boldsymbol{\phi}}_i^{\,T}\boldsymbol{\phi}_i + c_i\hat{\boldsymbol{\phi}}_i^{\,T}\hat{\boldsymbol{\phi}}_i - \boldsymbol{\phi}_i^T\hat{\boldsymbol{\phi}}_i + c_i\hat{\boldsymbol{\phi}}_i^{\,T}\hat{\boldsymbol{\phi}}_i = 0 \\
-2\hat{\boldsymbol{\phi}}_i^{\,T}\boldsymbol{\phi}_i + 2c_i\hat{\boldsymbol{\phi}}_i^{\,T}\hat{\boldsymbol{\phi}}_i = 0 \\
\Rightarrow c_i = \frac{\hat{\boldsymbol{\phi}}_i^{\,T}\boldsymbol{\phi}_i}{\hat{\boldsymbol{\phi}}_i^{\,T}\hat{\boldsymbol{\phi}}_i} = \frac{\hat{\boldsymbol{\phi}}_i^{\,T}\boldsymbol{\phi}_i}{\|\hat{\boldsymbol{\phi}}_i\|^2}
\end{aligned}$$

For our analysis, we normalize $\hat{\boldsymbol{\phi}}_i$ such that $\|\hat{\boldsymbol{\phi}}_i\|^2 = 1$ so finally the expression for the c_i is :

$$c_i = \hat{\boldsymbol{\phi}}_i^{\,T}\boldsymbol{\phi}_i \tag{5.7}$$

Minimization problem

Thus, returning to our original minimization problem we have to minimize the objective function :

$$J(\boldsymbol{\phi}, \lambda) = J(\boldsymbol{\phi}) + \lambda(1 - \boldsymbol{\phi}^T\boldsymbol{\phi}) = \sum_{i=1}^{n_s} \|\boldsymbol{\phi}_i - (\hat{\boldsymbol{\phi}}_i^{\,T}\boldsymbol{\phi}_i)\hat{\boldsymbol{\phi}}_i\|^2 + \lambda(1 - \boldsymbol{\phi}^T\boldsymbol{\phi}) \tag{5.8}$$

By substituting $\boldsymbol{\phi}_i = \boldsymbol{L}_i\boldsymbol{\phi}$ in the above equation we have :

$$\begin{aligned}
J(\boldsymbol{\phi}, \lambda) &= \sum_{i=1}^{n_s} \|\boldsymbol{L}_i\boldsymbol{\phi} - \hat{\boldsymbol{\phi}}_i\hat{\boldsymbol{\phi}}_i^{\,T}\boldsymbol{L}_i\boldsymbol{\phi}\|^2 + \lambda(1 - \boldsymbol{\phi}^T\boldsymbol{\phi}) \\
&= \sum_{i=1}^{n_s} \|(\boldsymbol{L}_i - \hat{\boldsymbol{\phi}}_i\hat{\boldsymbol{\phi}}_i^{\,T}\boldsymbol{L}_i)\boldsymbol{\phi}\|^2 + \lambda(1 - \boldsymbol{\phi}^T\boldsymbol{\phi}) \\
= \sum_{i=1}^{n_s} \boldsymbol{\phi}^T(\boldsymbol{L}_i - \hat{\boldsymbol{\phi}}_i\hat{\boldsymbol{\phi}}_i^{\,T}\boldsymbol{L}_i)^T(\boldsymbol{L}_i - \hat{\boldsymbol{\phi}}_i\hat{\boldsymbol{\phi}}_i^{\,T}\boldsymbol{L}_i)\boldsymbol{\phi} &+ \lambda(1 - \boldsymbol{\phi}^T\boldsymbol{\phi})
\end{aligned}$$

And in more compact form :

$$J(\boldsymbol{\phi}, \lambda) = \sum_{i=1}^{n_s} \boldsymbol{\phi}^T\boldsymbol{A}_i\boldsymbol{\phi} + \lambda(1 - \boldsymbol{\phi}^T\boldsymbol{\phi}) \tag{5.9}$$

Where we have defined $\boldsymbol{A}_i$ as :

$$\boldsymbol{A}_i = (\boldsymbol{L}_i - \hat{\boldsymbol{\phi}}_i \hat{\boldsymbol{\phi}}_i^{\,T} \boldsymbol{L}_i)^T (\boldsymbol{L}_i - \hat{\boldsymbol{\phi}}_i \hat{\boldsymbol{\phi}}_i^{\,T} \boldsymbol{L}_i) \tag{5.10}$$

A more careful examination of $\boldsymbol{A}_i$ yields :

$$\begin{aligned} \boldsymbol{A}_i &= (\boldsymbol{L}_i - \hat{\boldsymbol{\phi}}_i \hat{\boldsymbol{\phi}}_i^{\,T} \boldsymbol{L}_i)^T (\boldsymbol{L}_i - \hat{\boldsymbol{\phi}}_i \hat{\boldsymbol{\phi}}_i^{\,T} \boldsymbol{L}_i) \\ &= (\boldsymbol{L}_i^T - \boldsymbol{L}_i^T \hat{\boldsymbol{\phi}}_i \hat{\boldsymbol{\phi}}_i^{\,T}) (\boldsymbol{L}_i - \hat{\boldsymbol{\phi}}_i \hat{\boldsymbol{\phi}}_i^{\,T} \boldsymbol{L}_i) \\ = \boldsymbol{L}_i^T \boldsymbol{L}_i - \boldsymbol{L}_i^T \hat{\boldsymbol{\phi}}_i \hat{\boldsymbol{\phi}}_i^{\,T} \boldsymbol{L}_i - \boldsymbol{L}_i^T \hat{\boldsymbol{\phi}}_i \hat{\boldsymbol{\phi}}_i^{\,T} \boldsymbol{L}_i + \boldsymbol{L}_i^T \hat{\boldsymbol{\phi}}_i \hat{\boldsymbol{\phi}}_i^{\,T} \hat{\boldsymbol{\phi}}_i \hat{\boldsymbol{\phi}}_i^{\,T} \boldsymbol{L}_i \end{aligned}$$

Taking into account that we normalize our measured mode shapes, $\|\hat{\boldsymbol{\phi}}_i\|^2 = 1 \Rightarrow \hat{\boldsymbol{\phi}}_i^{\,T} \hat{\boldsymbol{\phi}}_i = 1$ we can further simplify the expression for $\boldsymbol{A}_i$:

$$\boldsymbol{A}_i = \boldsymbol{L}_i^T \boldsymbol{L}_i - \boldsymbol{L}_i^T \hat{\boldsymbol{\phi}}_i \hat{\boldsymbol{\phi}}_i^{\,T} \boldsymbol{L}_i \tag{5.11}$$

From equation (5.11) we can deduce that $\boldsymbol{A}_i \in R^{n \times n}$, $\boldsymbol{A}_i^T = \boldsymbol{A}_i$ and $\boldsymbol{A}_i$ is independent of $\boldsymbol{\phi}$. Thus, returning to our objective function we note from equation (5.9) that $J(\boldsymbol{\phi}, \lambda)$ is quadratic in $\boldsymbol{\phi}$ components, thus we expect to solve it analytically, using derivatives :

$$J(\boldsymbol{\phi}, \lambda) = \sum_{i=1}^{n_s} \boldsymbol{\phi}^T \boldsymbol{A}_i \boldsymbol{\phi} + \lambda(1 - \boldsymbol{\phi}^T \boldsymbol{\phi})$$

$$\Rightarrow \frac{\partial J}{\partial \phi_j} = \sum_{i=1}^{n_s} (\frac{\partial \boldsymbol{\phi}}{\partial \phi_j})^T \boldsymbol{A}_i \boldsymbol{\phi} + \boldsymbol{\phi}^T \boldsymbol{A}_i \frac{\partial \boldsymbol{\phi}}{\partial \phi_j} - \lambda(\frac{\partial \boldsymbol{\phi}^T}{\partial \phi_j} \boldsymbol{\phi} + \boldsymbol{\phi}^T \frac{\partial \boldsymbol{\phi}}{\partial \phi_j}) \tag{5.12}$$

Further simplification is achieved when noticing that the assembled modeshape vector $\boldsymbol{\phi}$ has constant elements, therefore the derivative of the vector with respect to a specific element is a zero-vector with only one non-zero element equal to one, in the position of the aforementioned derivation element.

$$\boldsymbol{\phi} = (\phi_1, \phi_2, \ldots, \phi_j, \ldots, \phi_n)^T \Rightarrow \frac{\partial \boldsymbol{\phi}}{\partial \phi_j} = (0, 0, \ldots, 1, \ldots, 0)^T$$

Using Kronecker's delta we can rewrite the derivative in a more compact form :

$$\frac{\partial \boldsymbol{\phi}}{\partial \phi_j} = \boldsymbol{\delta}_j \in R^n \tag{5.13}$$

By substituting into equation (5.12) we obtain :

$$\frac{\partial J}{\partial \phi_j} = \sum_{i=1}^{n_s} \boldsymbol{\delta}_j^T \boldsymbol{A}_i \boldsymbol{\phi} + \boldsymbol{\phi}^T \boldsymbol{A}_i \boldsymbol{\delta}_j - \lambda(\boldsymbol{\delta}_j^T \boldsymbol{\phi} + \boldsymbol{\phi}^T \boldsymbol{\delta}_j)$$

We notice that the terms of the resulting equation are scalar, and therefore they are equal to their transpose. Using the matrix identity : $(\mathbf{ABC})^T = \mathbf{C}^T \mathbf{B}^T \mathbf{A}^T$, and by using the fact that $\boldsymbol{A}_i^T = \boldsymbol{A}_i$ from equation (5.11), we further simplify the derivative to :

$$\frac{\partial J}{\partial \phi_j} = 2\sum_{i=1}^{n_s}(\boldsymbol{\delta}_j^T \boldsymbol{A}_i \boldsymbol{\phi}) - 2\lambda \boldsymbol{\delta}_j^T \boldsymbol{\phi} = 0 \ , \ \ j = 1, \ldots, n \tag{5.14}$$

Equations (5.14) form a system of n equations linear in $\boldsymbol{\phi}$. We can estimate $\boldsymbol{\phi}$ from its solution. Because of its linearity, this system of equations can be solved analytically. First we rewrite the equations in matrix form. To do that we note that the product $\boldsymbol{A}_i\boldsymbol{\phi}$ is a column vector of size n. Its pre-multiplication with $\boldsymbol{\delta}_j^T$ returns a scalar which is just the j^{th} element of $\boldsymbol{A}_i\boldsymbol{\phi}$. The same holds for the second term of equations (5.14). Therefore, the matrix form of the system is :

$$\sum_{i=1}^{n_s} \boldsymbol{A}_i\boldsymbol{\phi} - \lambda\boldsymbol{\phi} = \boldsymbol{0} \Rightarrow \boldsymbol{A}_0\boldsymbol{\phi} - \lambda\boldsymbol{\phi} = \boldsymbol{0} \Rightarrow \boldsymbol{A}_0\boldsymbol{\phi} = \lambda\boldsymbol{\phi} \ , \ \boldsymbol{A}_0 = \sum_{i=1}^{n_s} \boldsymbol{A}_i \tag{5.15}$$

Equation (5.15) constitutes an *eigenvalue* problem. This means that in order to find our unknown assembled mode shape $\boldsymbol{\phi}$ we have to find the eigenvectors of the matrix $\boldsymbol{A}_0$ given in the above equation. An obvious issue that we have to address is the multitude of eigenvectors. Specifically, since matrix $\boldsymbol{A}_0$ is of dimension $n \times n$ the solution of the eigenproblem will yield n eigenvectors, but we want one solution.

We choose the eigenvector $\boldsymbol{\phi}^{(r)}$ that minimizes our objective function $J(\boldsymbol{\phi}, \lambda)$:

$$J(\boldsymbol{\phi}, \lambda) = \sum_{i=1}^{n_s} \boldsymbol{\phi}^T \boldsymbol{A}_i \boldsymbol{\phi} + \lambda(1 - \boldsymbol{\phi}^T\boldsymbol{\phi}) = \boldsymbol{\phi}^T(\sum_{i=1}^{n_s} \boldsymbol{A}_i)\boldsymbol{\phi} + \lambda(1 - \boldsymbol{\phi}^T\boldsymbol{\phi})$$

$$\Rightarrow J(\boldsymbol{\phi}, \lambda) = \boldsymbol{\phi}^T\boldsymbol{A}_0\boldsymbol{\phi} + \lambda(1 - \boldsymbol{\phi}^T\boldsymbol{\phi}) \tag{5.16}$$

For the r^{th} eigenvector we have that : $\boldsymbol{A}_0\boldsymbol{\phi}^{(r)} = \lambda^{(r)}\boldsymbol{\phi}^{(r)}$ and we also assume that we have normalized the eigenvector such that $\|\boldsymbol{\phi}^{(r)}\|^2 = 1$

By substituting into the objective function we have :

$$J(\boldsymbol{\phi}^{(r)}, \lambda) = \boldsymbol{\phi}^{(r)T}\boldsymbol{A}_0\boldsymbol{\phi}^{(r)} = \boldsymbol{\phi}^{(r)T}\lambda^{(r)}\boldsymbol{\phi}^{(r)} = \lambda^{(r)}\boldsymbol{\phi}^{(r)T}\boldsymbol{\phi}^{(r)} = \lambda^{(r)}\|\boldsymbol{\phi}^{(r)}\|^2$$

$$\Rightarrow J(\boldsymbol{\phi}^{(r)}, \lambda) = \lambda^{(r)} \tag{5.17}$$

It is obvious that the objective function is minimized when $\lambda^{(r)}$ is minimum, i.e. the lowest eigenvalue of the problem. Therefore, the solution to the problem is the eigenvector that corresponds to the lowest eigenvalue, namely $\boldsymbol{\phi}^{(1)}$.

To sum up the important equations, first, we find $\boldsymbol{A}_i$ based on the configuration matrix $\boldsymbol{L}_i$ and the measurements $\hat{\boldsymbol{\phi}}_i$ from (5.11). Then we use equation (5.15) to find $\boldsymbol{A}_0$ from the $\boldsymbol{A}_i$ and find the eigenvalues and eigenvectors of $\boldsymbol{A}_0$. The eigenvector corresponding to the lowest eigenvalue is the solution to our problem.

Chapter 6

Optimal Sensor Location

In the previous chapter we investigated the problem of combining the measured mode shape components from reference setups into the global measured mode shape. However, the issue of choosing the locations of the sensors in the various setups has not been addressed yet. In this chapter, two methods for finding the optimal location of the reference sensors are presented. The first is heuristic and makes use of the visual representation of the mode shapes at the DOFs of the structure which are possible to be measured. The second is much more involved and makes use of the Information Entropy as a performance measure of a sensor configuration. The optimal sensor location is formulated as an optimization problem involving discrete-valued variables, which is solved using computationally efficient sequential sensor placement algorithms. The information entropy is used as a performance measure of the sensor configuration. A theoretical analysis [Papadimitriou and Lombaert 2011] shows that the spatial correlation length of the prediction errors controls the minimum distance between the sensors and should be taken into account when designing optimal sensor locations with potential sensor distances up to the order of the characteristic length of the dynamic problem considered. The optimal sensor location theory is demonstrated by designing the optimal reference locations for the Metsovo bridge.

6.1 Visual Inspection Method

The main idea of this method is to place the sensors in locations where we have the most active vibrations of as many modes as possible. The theoretical (FEM) model of the structure can be useful for that matter, in providing us with the plots of the mode shapes. Our main concern is to avoid placing sensors in nodal points because we wont be able to identify these modes in this specific point. On the contrary, the optimal points are the ones in which the most modes happen to have great (relative) deflection. An accelerometer placed in such a point will be able to identify all the modes (frequencies and mode shapes) that vibrate actively in that point. In the next figures we see plots of the mode shapes of the Metsovo bridge in the vertical and transverse direction.

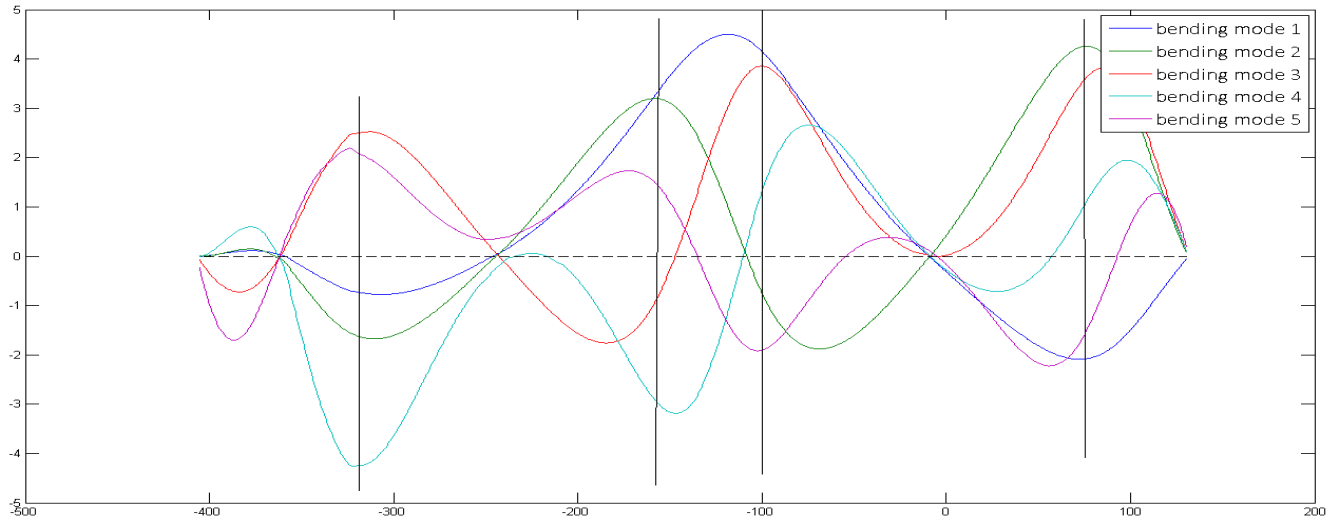

Figure 6.1: Bending modes (1-5)

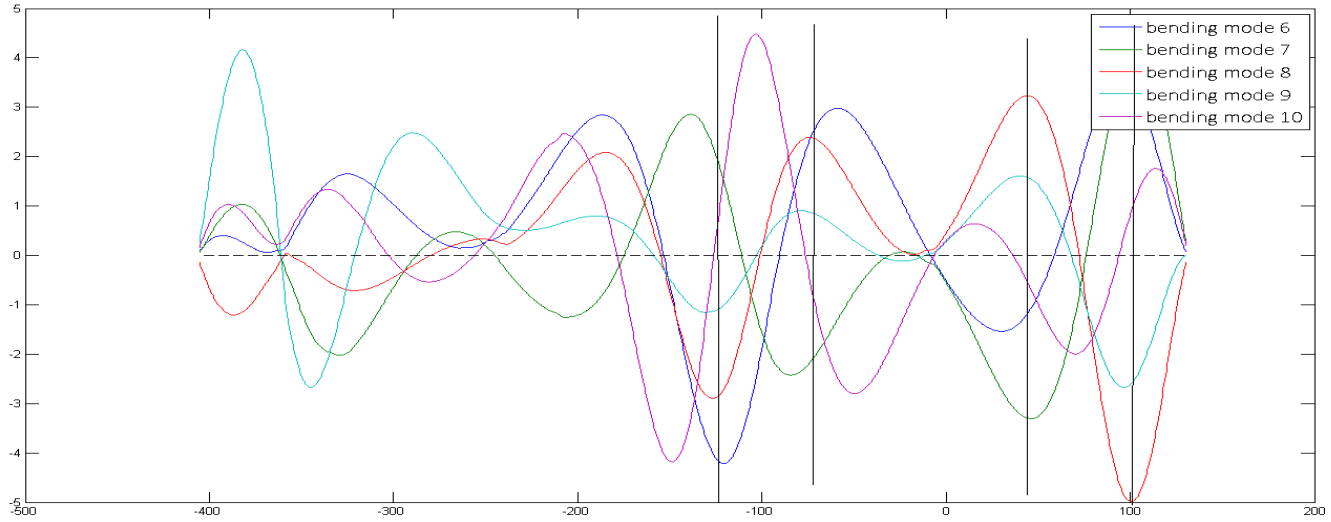

Figure 6.2: Bending modes (6-10)

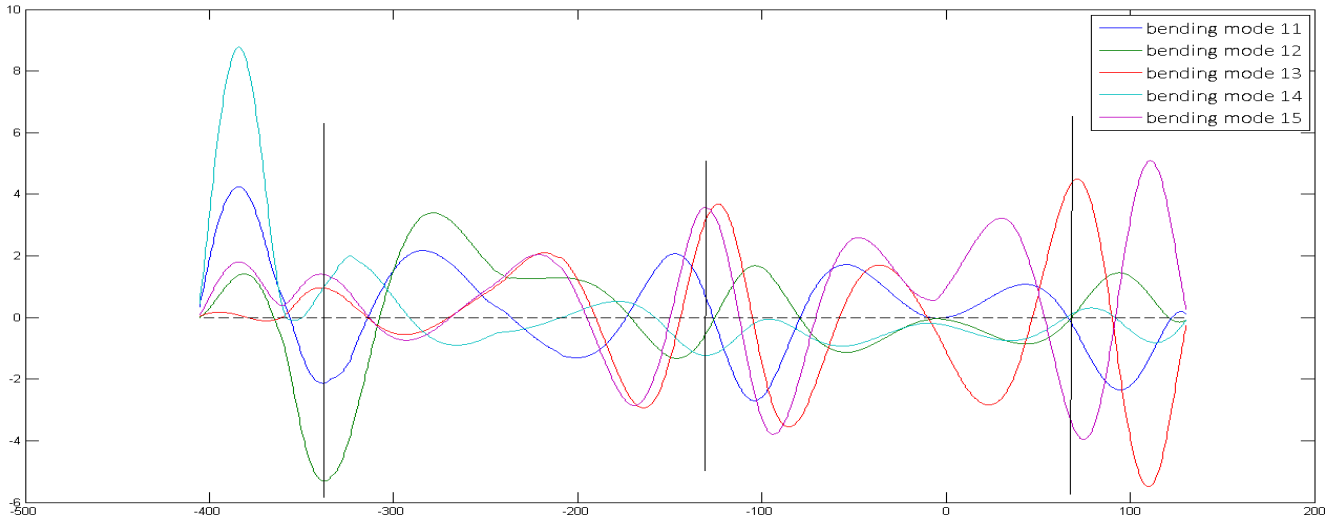

Figure 6.3: Bending modes (11-15)

Figure 6.4: Transverse modes (1-7)

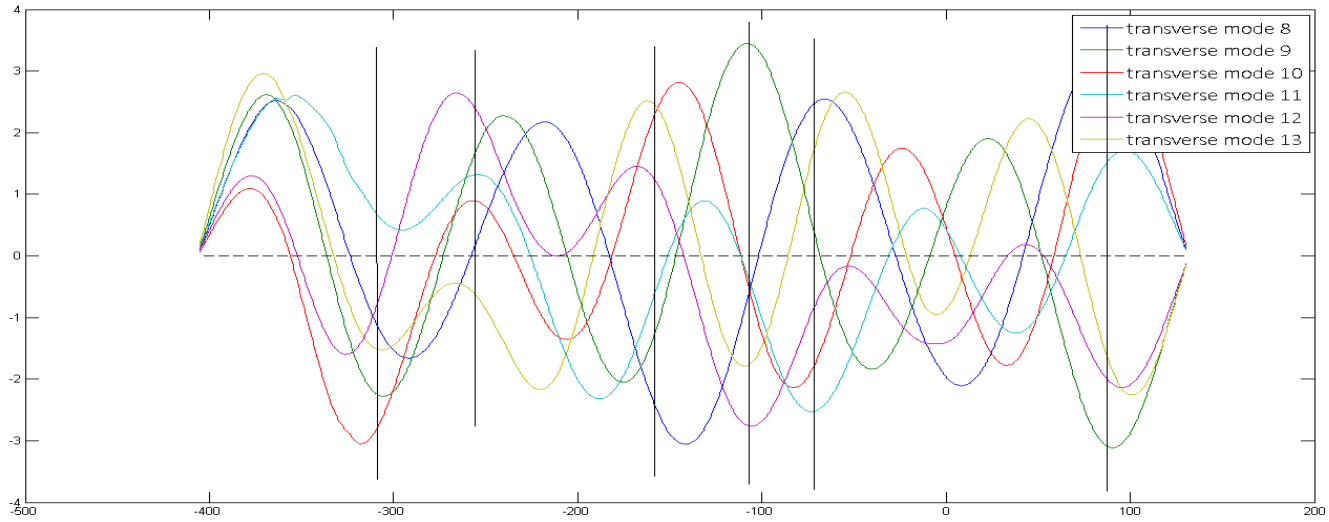

Figure 6.5: Transverse modes (8-13)

In the above figures, the horizontal axis is the x coordinate according to the FEM model of the bridge, which spans the total length of the bridge, a total of 537 m. The vertical axis is the mode shape component for the corresponding DOF in the vertical direction for the bending modes and in the transverse direction for the transverse modes. The vertical lines indicate possible sensor locations, e.g. the vertical line at $x = -310$ in Figure (6.5) corresponds to a sensor location at $d = -310-(-405) = 95m$ from the start of the deck. A fast way to select posotions for our reference sensors would be to place them in the positions indicated by the vertical lines in Figures (6.1)-(6.5) depending always on the modes we would like to identify with greater accuracy.

6.2 Information Entropy Method

6.2.1 Introduction

The main reason for which we want to find the optimal sensor location is to identify structural parameters (natural frequencies, mode shapes) in the most accurate way. The estimate of the parameter values involves uncertainties that are due to limitations of the mathematical models used to represent the behavior of the real structure, the presence of measurement error in the data and insufficient excitation and response bandwidth. In particular, the quality of information that can be extracted from the data for estimating the model parameters depends on the number and location of sensors in the structure as well as on the type and size of model and measurement error. The objective in an experimental design is to make a cost-effective selection of the optimal number and location of sensors such that the resulting measured data are most informative for estimating the parameters of a mathematical model of the structure.

Information theory based approaches have been developed to provide rational solutions to several issues encountered in the problem of selecting the optimal sensor configuration for modal identification and structural parameter estimation. The optimal sensor configuration is selected as the one that maximizes some norm (determinant or trace) of the Fisher information matrix (FIM) [Qureshi et al. 1980].

The information entropy, measuring the uncertainty in the model parameter estimates, was also introduced [Papadimitriou et al. 2000] for designing optimal sensor configurations. It was shown [Papadimitriou 2004] that, asymptotically for very large number of data, the information entropy depends on the determinant of the FIM, justifying the use of the determinant instead of the trace or other scalar measures of FIM in previous approaches. The optimal sensor location problem is formulated as a single-objective optimization problem involving discrete-valued variables. Computational efficient algorithms for solving the discrete-valued minimization problem have been proposed. Udwadia (1994) demonstrated that using the trace of the FIM is computationally very attractive since the solution of the underlined discrete optimization problem is straightforward. However, for other more popular scalar measures of uncertainties such as the determinant of the FIM or the information entropy, an exhaustive search over all possible sensor configurations is required to obtain the exact optimal sensor configuration. This approach is computationally prohibitive even for structures with a relatively small number of degrees of freedom (DOF). Heuristic optimization tools have also been developed as effective alternatives for efficiently solving these discrete optimization problems involving discrete-valued variables. In the modal identification case, exploiting theoretical asymptotic results on information entropy and FIM, two computationally efficient heuristic algorithms, the forward sequential sensor placement (FSSP) and the backward sequential sensor placement (BSSP) [Papadimitriou 2004, 2005] were proposed. These algorithms construct sensor configurations for physical model parameter estimation, corresponding to information entropy values very close to lower or upper bounds of the information entropy.

In most information theory-based methods the effect of spatially correlated prediction errors and its importance was not adequately explored. The present study provides insight into the effect of spatially correlated prediction errors on the design of the optimal sensor locations. The information entropy is used as the performance measure of a sensor configuration. The information entropy is built from the parameter uncertainty identified by applying a Bayesian identification framework. The optimal sensor location problem is formulated as a single-objective optimization problem involving discrete-valued variables. The effectiveness of available heuristic algorithms BSSP and FSSP, known to be computationally very efficient and accurate for uncorrelated prediction errors, is explored.

Asymptotic approximations, valid for large number of data, available for the information entropy [Papadimitriou 2004] for the case of uncorrelated prediction errors are extended to account for the case of spatially correlated prediction errors. Useful theoretical results are derived that show that the lower and upper bounds of the asymptotic estimate of the information entropy, corresponding, respectively, to the optimal and worst sensor configuration, are a decreasing function of the number of sensors. In addition, it is shown that for up to the characteristic length of the highest contributing mode of the structure, the spatial correlation between prediction errors forces the minimum distance between sensors to be of the order of the prediction error correlation length. Consequently, sensor placement becomes independent of the mesh size of the finite element models used for structural dynamics simulations. For distances between two sensors higher than the characteristic length, the sensor locations are affected also by the spatial variability of the response sensitivities computed by a nominal structural model. Implementation in structural dynamics is concentrated on the design of optimal sensor location for (a) modal identification and (b) estimation of structural model (e.g. finite element) parameters.

6.2.2 Estimation of model parameter uncertainty

Bayesian statistical framework

Consider a parameterized class of structural models (e.g. a class of finite element models or a class of modal models) chosen to describe the input–output behavior of a structure. Let $\boldsymbol{\theta} \in R^{N_\theta}$ be the vector of free parameters (physical or modal parameters) in the model class that need to be estimated using measured data D collected from a sensor network. Let $D = \{\boldsymbol{y}_k, k = 1, \ldots, N\}$ be the measured sampled response time histories data, where $\boldsymbol{y}_k \in R^{N_0}$ refer to output data, N_0 is the number of observed DOFs of the structural model, k denotes the time index at time $k\Delta t$, Δt is the sampling interval and N is the number of sampled data. Let $\boldsymbol{x}_k(\boldsymbol{\theta}) \in R^{N_d}$, $k = 1, \ldots, N$ be the sampled response time histories computed at all N_d model DOFs from a structural model that corresponds to a specific value $\boldsymbol{\theta}$ of the model parameters.

The measured response and model response predictions at time instant $k\Delta t$ satisfy the prediction error equation:

$$\boldsymbol{y}_k = \boldsymbol{L}\boldsymbol{x}_k(\boldsymbol{\theta}) + \boldsymbol{L}\boldsymbol{e}_k(\boldsymbol{\theta}) \tag{6.1}$$

where $\boldsymbol{e}_k(\boldsymbol{\theta})$ is the prediction error due to modeling error and measurement noise. The matrix $\boldsymbol{L} \in R^{N_0 \times N_d}$ is the observation matrix comprised of zeros and ones and maps the model DOFs to the measured DOFs. The matrix L therefore defines the location of the sensors in the structure.

Using a Bayesian identification methodology [Beck and Katafygiotis 1998] and [Katafygiotis et al. 1998], the uncertainties in the values of the parameters $\boldsymbol{\theta}$ are quantified by probability density functions (PDF) that are obtained using the dynamic test data D and the probability model for the prediction error $\boldsymbol{e}_k(\boldsymbol{\theta})$. In what follows, the prediction error vector $\boldsymbol{e}_k(\boldsymbol{\theta})$ at time $k\Delta t$ is modeled as a Gaussian random vector with zero mean and covariance $\boldsymbol{\Sigma}_t \in R^{N_d \times N_d}$. Also, it is assumed that the prediction errors between different time instances are independent. Applying Bayes' theorem, the updating PDF $p(\boldsymbol{\theta}|\boldsymbol{\Sigma}_t, D)$ of the set of structural model parameters $\boldsymbol{\theta}$ given the measured data D and the prediction error parameters $\boldsymbol{\Sigma}_t$ takes the form:

$$p(\boldsymbol{\theta}|\boldsymbol{\Sigma}_t, D) = c\frac{1}{(\sqrt{2\pi})^N \sqrt{det\boldsymbol{\Sigma}_t}} exp[-\frac{NN_0}{2} J(\boldsymbol{\theta};\, \boldsymbol{\Sigma}_t, D)]\pi(\boldsymbol{\theta}) \tag{6.2}$$

where

$$J(\boldsymbol{\theta};\, \boldsymbol{\Sigma}_t, D) = \frac{1}{NN_0} \sum_{k=1}^{N} [\boldsymbol{y}_k - \boldsymbol{L}\boldsymbol{x}_k(\boldsymbol{\theta})]^T \boldsymbol{\Sigma}_t^{-1} [\boldsymbol{y}_k - \boldsymbol{L}\boldsymbol{x}_k(\boldsymbol{\theta})] \tag{6.3}$$

represents the measure of fit between the measured and the model response time histories, $\pi(\boldsymbol{\theta})$ is the prior distribution for the parameter set $\boldsymbol{\theta}$ and c is a normalizing constant chosen such that the PDF in (6.2) integrates to one.

Prediction error correlation model

An analysis of the prediction error correlation models is presented next. The prediction error $\boldsymbol{e}_k = \boldsymbol{e}_{k,meas} + \boldsymbol{e}_{k,mod}$ in (6.1) is due to a term, $\boldsymbol{e}_{k,meas}$ accounting for the measurement error and a term, $\boldsymbol{e}_{k,mod}$ accounting for the model error. Assuming independence between the measurement error and model error, the covariance $\boldsymbol{\Sigma}_t$ of the total prediction error is given in the form:

$$\boldsymbol{\Sigma}_t = \overline{\boldsymbol{\Sigma}} + \boldsymbol{\Sigma} \tag{6.4}$$

where $\overline{\boldsymbol{\Sigma}}$ and $\boldsymbol{\Sigma}$ are the covariance matrices of the measurement and model errors, respectively.

The designer has to assume values for the individual covariance matrices in (6.4). Such assumptions may depend on the nature of the problem analyzed. One reasonable choice is to assume that the measurement error is independent of the location of sensors so that the covariance $\overline{\boldsymbol{\Sigma}}$ takes the diagonal form $\overline{\boldsymbol{\Sigma}} = s^2 I$, where I is the identity matrix. However, a certain degree of correlation should be expected for the

model errors between two neighborhood locations arising from the underlining model dynamics. This correlation can be taken into account by selecting a non-diagonal covariance matrix $\mathbf{\Sigma}$.

The correlation Σ_{ij} between the prediction errors $\epsilon_{i,mod}$ and $\epsilon_{j,mod}$ at DOFs i and j, respectively, is given by:

$$\Sigma_{ij} = E[\epsilon_{i,mod}\epsilon_{j,mod}] = \sqrt{\Sigma_{ii}\Sigma_{jj}}R(\delta_{ij}) \tag{6.5}$$

that accounts for the spatial distance δ_{ij} between the DOFs i and j, where $R(\delta_{ij})$ is a correlation function satisfying $R(0) = 1$. In general, the covariance matrix should be consistent with the actual errors and correlations as observed from measurements. However, in an experimental design stage such measurements are not available to guide the selection of the correlation between prediction errors. Instead a correlation function should be postulated to proceed with the design of the optimal sensor locations. Several correlation functions can be explored. For demonstration purposes in this study, the following exponential correlation function is assumed:

$$R(\delta) = exp[-\frac{\delta}{\lambda}] \tag{6.6}$$

where λ is a measure of the spatial correlation length. However, the formulation in this work is general and does not depend on the choice of the correlation model.

6.2.3 Optimal sensor location methodology

Asymptotic estimate of the information entropy

The updated PDF $p(\boldsymbol{\theta}|\mathbf{\Sigma}_t, D)$ given in (6.2) represents the uncertainty in the structural model parameter values based on the information contained in the measured data. The information entropy, defined by:

$$h(\boldsymbol{L};\, \mathbf{\Sigma}, D) = E_{\boldsymbol{\theta}}[-ln\, p(\boldsymbol{\theta};\, \mathbf{\Sigma}, D)] = -\int ln\, p(\boldsymbol{\theta}|\mathbf{\Sigma}, D)p(\boldsymbol{\theta}|\mathbf{\Sigma}, D)d\boldsymbol{\theta} \tag{6.7}$$

has been introduced [Papadimitriou et al. 2000] to provide a unique scalar measure of the uncertainty in the estimate of the structural parameters $\boldsymbol{\theta}$. The information entropy depends on the available data $D \equiv D(\boldsymbol{L})$ and the sensor configuration vector $\boldsymbol{L}$.

An asymptotic approximation of the information entropy, valid for large number of data ($NN_0 \to \infty$), is available [Papadimitriou 2004] which is useful in the experimental stage of designing an optimal sensor configuration. The asymptotic approximation is obtained by substituting $p(\boldsymbol{\theta}|\mathbf{\Sigma}_t, D)$ from (6.2) into (6.7) and observing that the resulting integral can be re-written as a Laplace-type integral, which can be approximated by applying Laplace method of asymptotic approximation [Bleistein and Handelsman 1986].

Specifically, it can be shown that for a large number of measured data, i.e. as $NN_0 \to \infty$, the following asymptotic result holds for the information entropy [Papadimitriou 2004]:

$$h(\boldsymbol{L};\, \boldsymbol{\Sigma}, D) \sim h(\boldsymbol{L};\, \boldsymbol{\Sigma}, \boldsymbol{\theta}_0) = \frac{1}{2} N_\theta ln(2\pi) - \frac{1}{2} ln[det\, Q(\boldsymbol{L};\, \boldsymbol{\theta}_0, \boldsymbol{\Sigma})] \tag{6.8}$$

where $\boldsymbol{\theta}_0 \equiv \widehat{\boldsymbol{\theta}}(\boldsymbol{L}, \boldsymbol{\Sigma}, D)$ is the optimal value of the parameter set $\boldsymbol{\theta}$ that minimizes the measure of fit $J(\boldsymbol{\theta};\, \boldsymbol{L}, D)$ given in (6.3), and $Q(\boldsymbol{L};\, \boldsymbol{\theta}, \boldsymbol{\Sigma})$ is an $N_\theta \times N_\theta$ semi-positive definite matrix defined as $NN_0\, \nabla_{\boldsymbol{\theta}} \nabla_{\boldsymbol{\theta}}^T\, J(\boldsymbol{\theta};\, \boldsymbol{\Sigma}, D)$ and asymptotically approximated by:

$$Q(\boldsymbol{L};\, \boldsymbol{\theta}, \boldsymbol{\Sigma}) = \sum_{k=1}^{N} (\boldsymbol{L} \nabla_{\boldsymbol{\theta}} \boldsymbol{x}_k)^T (\boldsymbol{L} \boldsymbol{\Sigma} \boldsymbol{L}^T)^{-1} (\boldsymbol{L} \nabla_{\boldsymbol{\theta}} \boldsymbol{x}_k) \tag{6.9}$$

in which $\nabla_{\boldsymbol{\theta}} = [\frac{\partial}{\partial \theta_1}, \ldots, \frac{\partial}{\partial \theta_{N_\theta}}]^T$ is the usual gradient vector with respect to the parameter set $\boldsymbol{\theta}$. For convenience the following notation was introduced $\nabla_{\boldsymbol{\theta}} \boldsymbol{x}_k \equiv \nabla_{\boldsymbol{\theta}} \boldsymbol{x}_k(\boldsymbol{\theta})$. The matrix $Q(\boldsymbol{L}, \boldsymbol{\theta}, \boldsymbol{\Sigma})$ is a semi-positive definite matrix, known as the Fisher Information Matrix (FIM), containing the information about the uncertainty in the values of the parameters $\boldsymbol{\theta}$ based on the data from all measured positions specified in $\boldsymbol{L}$. Details for the derivation in the special case of diagonal covariance matrix $\boldsymbol{\Sigma} = \sigma^2 \boldsymbol{I}$, where $\boldsymbol{I}$ is the identity matrix can be found in [Papadimitriou 2004].

In the initial stage of designing the experiment, the data and consequently the values of the optimal model parameters $\widehat{\boldsymbol{\theta}}$ and the form of the prediction error covariance matrix $\boldsymbol{\Sigma}$ are not available. In practice, useful designs can be obtained by taking the optimal model parameters $\widehat{\boldsymbol{\theta}}$ and prediction error covariance $\boldsymbol{\Sigma}$ to have some nominal values $\boldsymbol{\theta}_0$ and $\boldsymbol{\Sigma}$ to arise from a correlation function such as (6.6), chosen by the designer to be representative of the system and the expected model and measurement errors.

Formulation as a discrete-valued optimization problem

In experimental design, the sensors are placed in the structure such that the resulting measured data are most informative about the parameters of the model class used to represent the structure behavior. Since the information entropy gives the amount of useful information contained in the measured data, the optimal sensor configuration is selected as the one that minimizes the information entropy [Papadimitriou et al. 2000]. That is

$$\boldsymbol{L}_{best} = argmin_{\boldsymbol{L}}\, H(\boldsymbol{L};\, \boldsymbol{\theta}_0, \boldsymbol{\Sigma}) \tag{6.10}$$

where $H(\boldsymbol{L};\, \boldsymbol{\theta}_0, \boldsymbol{\Sigma})$ is given by (6.8) and the minimization is constrained over the set of N_p measurable DOFs. The lower bound of the information entropy is then given by $H_{min} = H(\boldsymbol{L}_{best};\, \boldsymbol{\theta}_0, \boldsymbol{\Sigma})$.

It should be noted that the upper bound of the information entropy corresponding to the worst sensor configuration is also useful since, when it is compared with the minimum information entropy for the same number of sensors, it gives a measure of the reduction that can be achieved by optimizing the sensor configuration.

The maximum information entropy and the corresponding worst sensor configuration can be obtained by maximizing instead of minimizing the information entropy. The worst sensor configuration is obtained as

$$\boldsymbol{L}_{worst} = argmax_{\boldsymbol{L}}\, H(\boldsymbol{L};\, \boldsymbol{\theta}_0, \boldsymbol{\Sigma}) \tag{6.11}$$

while the upper bound of the information entropy is given by $H_{max} = H(\boldsymbol{L}_{worst};\, \boldsymbol{\theta}_0, \boldsymbol{\Sigma})$.

Computational algorithms

Two heuristic sequential sensor placement (SSP) algorithms, the forward (FSSP) and the backward (BSSP), were proposed [Papadimitriou 2004, 2005] for constructing predictions of the optimal and worst sensor configurations. According to FSSP (Algorithm 1), the positions of N_0 sensors are computed sequentially by placing one sensor at a time in the structure at a position that results in the highest reduction in information entropy. BSSP (Algorithm 2) is used in an inverse order, starting with N_d sensors placed at all DOFs of the structure and removing successively one sensor at a time from the position that results in the smallest increase in the information entropy.

6.2.4 Analysis of information entropy

Dependence of information entropy on the number of sensors

Useful results are shown next that demonstrate how the information entropy and its lower and upper bounds depend on the number of sensors. The proofs can be found in Papadimitriou and Lombaert (2011). Let $\boldsymbol{L}_M$ denote the sensor configuration involving M sensors. Define also the expression $\boldsymbol{L}_{M+N} = (\boldsymbol{L}_M^T, \boldsymbol{L}_N^T)^T$ to represent the sensor configuration that is formed from the configuration $\boldsymbol{L}_M$ and N additional sensors placed on the structure as specified by the configuration $\boldsymbol{L}_N$. Then, the following proposition holds:

Proposition 1 : *The information entropy for a sensor configuration $\boldsymbol{L}_M$ involving M sensors is higher than the information entropy for a sensor configuration $\boldsymbol{L}_{M+N}$ involving N additional sensors. That is*

$$H(\boldsymbol{L}_{M+N};\, \boldsymbol{\theta}_0, \boldsymbol{\Sigma}) \leq H(\boldsymbol{L}_M;\, \boldsymbol{\theta}_0, \boldsymbol{\Sigma}) \tag{6.12}$$

Proposition 1 implies that the information entropy reduces as additional sensors are placed in a structure. Given the interpretation of the information entropy as a measure of the uncertainty in the parameter estimates, this should be intuitively expected since adding one or more sensors in the structure will have the effect of providing more information about the system parameters and thus reducing the uncertainty in the parameter estimates. As a direct consequence of Proposition 1, the following proposition is also true.

Proposition 2 : *The minimum and maximum information entropies for M sensors are decreasing functions of the number of sensors, M.*

This reduction of the information entropy as a function of the number of sensors is expected since increasing the number of sensors has the effect of extracting more information from the data. Proposition 2 follows directly from Proposition 1, independent of the correlation model assumed for the prediction error. Thus, the reader is referred to Papadimitriou (2004) for a proof.

Effect of correlation length on the distance between sensors

Let $\boldsymbol{L}_M$ be a sensor configuration involving M sensors that have already been placed on the structure. Let also Δ be the minimum distance between any two sensors in the sensor configuration $\boldsymbol{L}_M$. It is assumed that the correlation length λ of the prediction error is small enough compared to the minimum distance Δ between any two sensors in $\boldsymbol{L}_M$. This is sufficient to guarantee that the prediction errors between the responses at any two sensors in $\boldsymbol{L}_M$ are uncorrelated. Consider a new sensor to be placed on the structure and let δ be the distance of the new sensor from one of the existing sensors in $\boldsymbol{L}_M$. Without loss of generality it can be assumed that the new sensor will be placed closer to the M_{th} sensor in the configuration. Otherwise, the sensor numbering can be re-arranged such that the sensor the closest to the new sensor is the M_{th} sensor. The sensor location for the new sensor is defined by $\boldsymbol{L}_1 \in R^{1\times N_d}$. Consider that δ varies from values of zero up to the order of the correlation length λ so that, using the fact that λ is small compared to Δ, the prediction error at the position of the additional sensor is correlated to the closest M_{th} sensor and uncorrelated to the prediction errors from all other $M-1$ sensors in the sensor configuration $\boldsymbol{L}_M$. Let $\widehat{H}(\delta) \equiv H_\delta(\boldsymbol{L}_{M+1};\, \boldsymbol{\theta}_0, \boldsymbol{\Sigma})$ denote the information entropy as a function of the distance δ for $M+1$ sensors located according to the sensor configuration $\boldsymbol{L}_{M+1} = (\boldsymbol{L}_M^T, \boldsymbol{L}_1^T)^T$. Similarly let also $\widehat{Q}(\delta) \equiv Q_\delta(\boldsymbol{L}_{M+1};\, \boldsymbol{\theta}_0, \boldsymbol{\Sigma})$ denote the corresponding information matrix.

Proposition 3 : *Consider the problem of placing an additional sensor on a structure instrumented with M sensors. The information entropy for the sensor configuration $\boldsymbol{L}_{M+1}$ involving $M+1$ sensors is a decreasing function of the sortest distance δ of the new sensor from the other M sensors, provided that δ is sufficiently small. Mathematically, this proposition reads :*

$$\widehat{H}(\delta_1) < \widehat{H}(\delta_2) \;\; for\, any \;\; \delta_1 > \delta_2 \tag{6.13}$$

or, equivalently, using (6.8)

$$det\, \widehat{Q}(\delta_1) > det\, \widehat{Q}(\delta_2) \;\; for\, any \;\; \delta_1 > \delta_2 \tag{6.14}$$

where δ_1 and δ_2 are sufficiently small.

The proof of Proposition 3 is presented in Papadimitriou and Lombaert (2011) and shows that the proposition holds for distances δ smaller than the characteristic length of the structural dynamic problem under consideration. Considering that the response is a superposition of structural modes, this length is controlled by the characteristic length of the highest contributing mode which defines the length scale over which the response sensitivities with respect to the parameters fluctuate in space.

Expression (6.13) or (6.14) implies that sensors locations further away from an existing sensor have a higher information content. Consequently, the spatial correlation of the prediction error tends to shift a sensor away from existing sensor locations. Over a distance larger than the characteristic length, the spatial change of the response sensitivity will eventually control how far away the new sensor is placed from the existing ones.

6.2.5 Implementation in structural dynamics

The optimal sensor location methodology is implemented for applications in structural dynamics. For a linear structural model, arising from the discretization of continuous domain using the finite element method, the governing equations of motion are:

$$M\ddot{\boldsymbol{u}}(t) + C\dot{\boldsymbol{u}}(t) + K\boldsymbol{u}(t) = \Gamma \boldsymbol{z}(t) \tag{6.15}$$

where $M \in R^{N_d \times N_d}$, $C \in R^{N_d \times N_d}$ and $K \in R^{N_d \times N_d}$ are the mass, damping and stiffness matrices, respectively, $\boldsymbol{u}(t) \in R^{N_d}$ is the displacement response vector, $\boldsymbol{z}(t) \in R^{N_1}$ is the vector of independent input forces and $\Gamma \in R^{N_d \times N_1}$ is the input selection matrix. The measured response quantities are assumed to be either displacements, or velocities, or absolute accelerations with the sampled measured response $\boldsymbol{x}_k \in R^{N_d}$ given, respectively, by either $\boldsymbol{u}_k$, or $\dot{\boldsymbol{u}}_k$ or $\ddot{\boldsymbol{u}}_k$. Strain measurements can readily be accommodated in the formulation. The optimal sensor location design depends on the type of parameters considered for estimation.

Design of optimal sensor locations for modal identification

This category deals with the estimation of the modal coordinate vector $\boldsymbol{\xi} \in R^m \, (m \leq N_d)$ encountered in modal identification. The objective is to design the sensor configuration that provides the most information in order to estimate the modal coordinate vector $\boldsymbol{\xi}$. In this case, the parameter set $\boldsymbol{\theta} \equiv \boldsymbol{\xi}$. Following the conventional modal analysis, the response vector $\boldsymbol{x} \in R^{N_d}$ is given with respect to the parameter set $\boldsymbol{\theta}$ in the form $\boldsymbol{x} = \Phi\boldsymbol{\theta}$, where $\Phi \in R^{N_d \times m}$ is the mode shape matrix for m contributing modes. Noting that $\nabla_{\boldsymbol{\theta}}\boldsymbol{x} = \Phi$ and substituting into (6.9), the information matrix takes the form:

$$Q(\boldsymbol{L}, \boldsymbol{\theta}_0, \boldsymbol{\Sigma}) \equiv Q(\boldsymbol{L}, \boldsymbol{\Sigma}) = (\boldsymbol{L}\Phi)^T(\boldsymbol{L}\boldsymbol{\Sigma}\boldsymbol{L}^T)^{-1}(\boldsymbol{L}\Phi) \tag{6.16}$$

which is independent of the nominal parameter values $\boldsymbol{\theta}_0$. In addition, the optimal sensor locations are independent of the excitation used.

Based on the form of (6.16), a non-singular FIM matrix $Q(\boldsymbol{L}, \boldsymbol{\Sigma})$ is obtained only if the number of sensors, N_0, is at least equal to the number of contributing modes, m, or the number of parameters, $N_\theta \, (N_\theta = m)$. Otherwise, for $N_0 < m$, the matrix $Q(\boldsymbol{L}, \boldsymbol{\Sigma})$ in (6.16) is singular and the determinant of the FIM will be zero for any sensor configuration. Thus, for $N_0 < m$, the optimal sensor location problem cannot be performed. This means that the information content in the measured data is not sufficient to estimate all the parameters simultaneously. The problem is critical for the FSSP algorithm where one starts with no sensors placed on the structure

and sequentially adds one sensor at a time on the structure. The estimation of the sensor locations will be a problem for a small number of sensors, $N_0 < m$, and will considerably affect the optimal sensor location for $N_0 \geq m$. One way to optimally place sensors in the structure for $N_0 < m$ is to maximize the product of the N_0 non-zero eigenvalues of the FIM, instead of maximizing the product of all eigenvalues. This procedure allows to systematically and optimally place sensors in the structure even for the unidentifiable case that arises for a small number of sensors. This procedure considerably improves the FSSP estimates for $N_0 \geq m$.

6.2.6 Formulation in continuous space

Until this point the problem of optimal sensor locations has been formulated as a discrete optimization problem, because the design variables where the degrees of freedom of the structure which are discrete quantities. However, the main problem with this approach is the great computational cost of the optimization methods. An exhaustive search method that tries all combinations of sensor locations is computationally very expensive, and for systems with large number of DOFs is prohibitive. Heuristic methods such as Sequential Sensor Placement (SSP) methods are computationally very efficient but will not find the optimal solution. On the contrary, optimization methods for continuous systems are computationally much more efficient than for discrete systems.

When optimizing in the physical (continuous) space, the structure occupies a 3D domain and sensors can be placed on the 2D surface or 1D line. The physical space is the 2D (or 1D) surface of the domain of the structure. The design variables are the coordinates of the sensor locations in the physical 2D (or 1D) space instead of the DOF number.

In order to perform the optimization efficiently, the 2D surface or line must be smooth enough. In general, the mesh of the geometry of the structure will be complicated. For this reason we first map the complicated surface or line into a parent plane surface (parent straight line) and perform optimization over the parent plane surface (parent straight line). Then we use stochastic optimization methods that handle multiple local/global optima, e.g. the CMA method (Covariance Matrix Adaption).

However, in real applications there are also more practical restraints as to where we can place our sensors that must be considered. In the structure considered in this thesis, which is the Metsovo Bridge, the following restrictions hold true. Due to limited access, placing sensors in the piers of the bridge is not possible. Thus, sensors can be placed only in the deck of the bridge. This eliminates the vertical (z) direction from being optimized. Also, due to traffic limitations, the whole width of the deck is not accessible. Only the two edges of the deck (corresponding to the minimum and maximum values of the transverse direction) are available for sensor placement. These restrictions limit our minimization problem to two edges, as seen in the following figure.

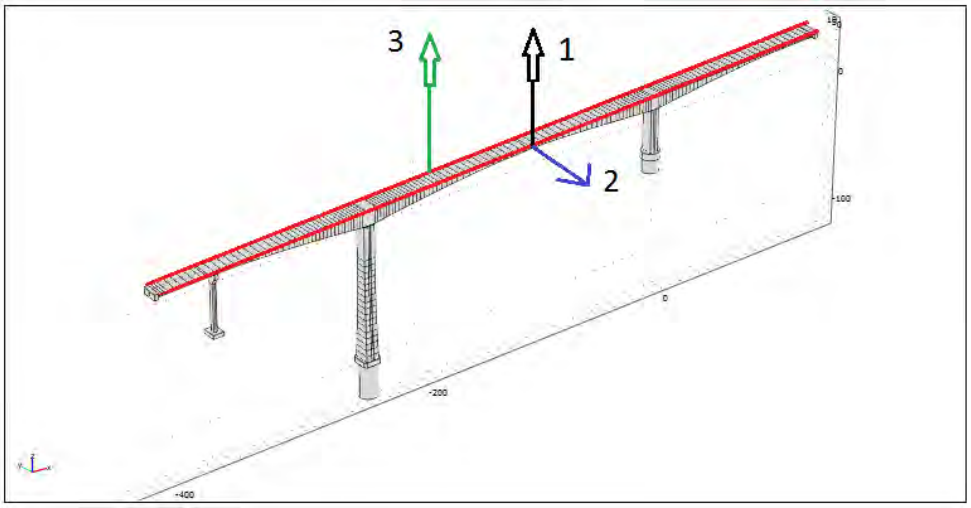

Figure 6.6: Optimization domains

Since our domains to be optimized are 1D curved lines (curved because of the slope of the deck), the parent domain will be a straight line. The three chosen domains are as follows:

1. Right edge, vertical direction (black)
2. Right edge, transverse direction (blue)
3. Left edge, vertical direction (green)

Therefore, our parent domain is defined as follows:

$$\xi \in [0, 3] \tag{6.17}$$

where

$$\begin{aligned} \xi \in [0,1] \; & maps\, to\, the\, x\, coordinates\, of\, the\, right\, edge\, (first\, domain) \\ \xi \in [1,2] \; & maps\, to\, the\, x\, coordinates\, of\, the\, right\, edge\, (second\, domain) \\ \xi \in [2,3] \; & maps\, to\, the\, x\, coordinates\, of\, the\, left\, edge\, (third\, domain) \end{aligned} \tag{6.18}$$

Note that the DOFs assigned to each domain are different, despite of the domains occupying the same physical space (domains 1 and 2).

The mode shapes required for the Optimal Sensor Location (OSL) software are known from the solution of the FEM program used (COMSOL). The software can optimize the sensor locations in the entire region, $\xi \in [0, 3]$ or we can specify which segments of ξ we would like to optimize for. There is also the possibility of adjusting the value of the spatial correlation length λ introduced in equation (6.6) and obtain interesting results. It seems that the correlation length λ plays an important role in the optimal placement of the sensors. An intuitive explanation for this is the following.

A zero value of the spatial correlation length, $\lambda = 0$ implies that the prediction errors are uncorrelated. Physically this means that two sensors placed in an infinitesimal distance apart will yield totally uncorrelated prediction errors. Therefore, we could obtain entirely different information content from these two sensors. But this is not a realistic situation because the modeling error in a point can not be uncorrelated with the modeling error in a point right next to it. A certain amount of correlation is expected, thus the information content from the adjacent sensor will be similar to its neighboring sensor. This is quantified by the spatial correlation length λ. The larger this value is, the greater the distance within which two sensors provide similar information content. Enlarging the value of λ leads to the optimal sensor locations moving away from each other, because in closer distances they provide no different information. This avoids the problem of sensor clustering, which occurs when assuming spatially uncorrelated prediction errors.

The issue of deciding the correct value for the spatial correlation length λ is discussed in Papadimitriou and Lombaert (2011), where it is shown that the value of λ should not be less than the characteristic length of the highest contributing mode because for distances smaller than that sensors tend to provide similar information content. Therefore, unacceptable designs with very close sensors are avoided by selecting the correlation length of the prediction errors to be at least of the order of the characteristic length of the problem.

6.2.7 Application for the Metsovo Bridge

This section presents the application of the Optimal Sensor Location theory outlined in the previous sections for the Metsovo Bridge. This task was performed using special Optimal Sensor Location software. This software takes as input the finite element mesh of the structure, including the nodes, DOFs, coordinates and mode-shapes, and returns as output the optimal locations for placing our sensors in the parent domain. Then the solution is transfered to the physical domain and plotted along with the mode shapes for visual confirmation and analysis of the results. The software is also capable of limiting the range of search for optimal sensor locations to account for practical limitations often encountered in real field measurements.

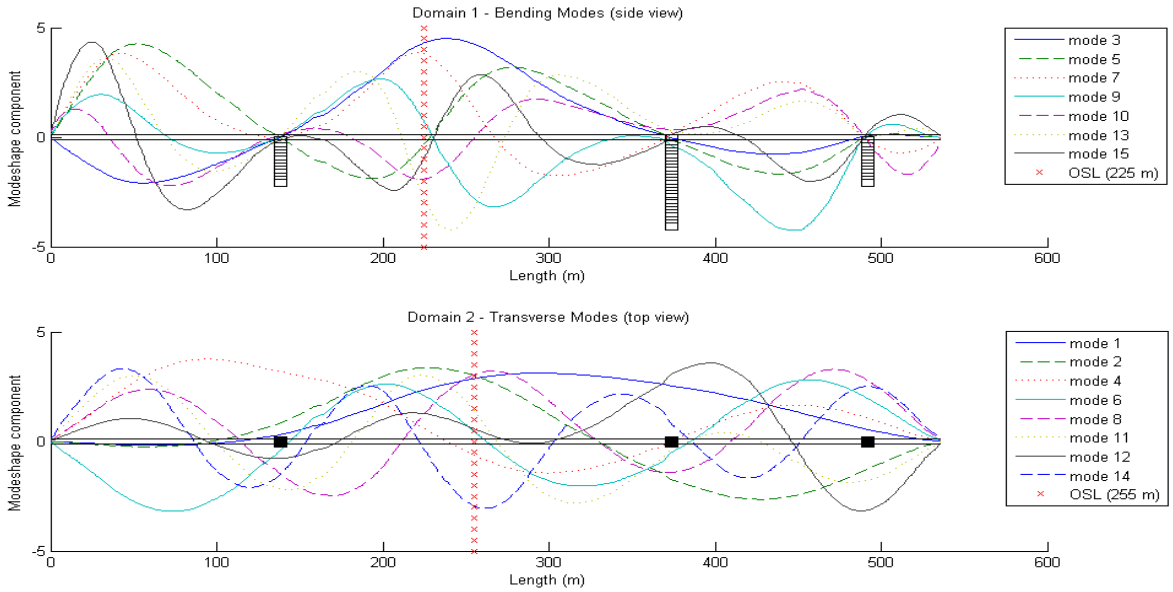

Figure 6.7: Optimal Sensor Locations for modes 1-15

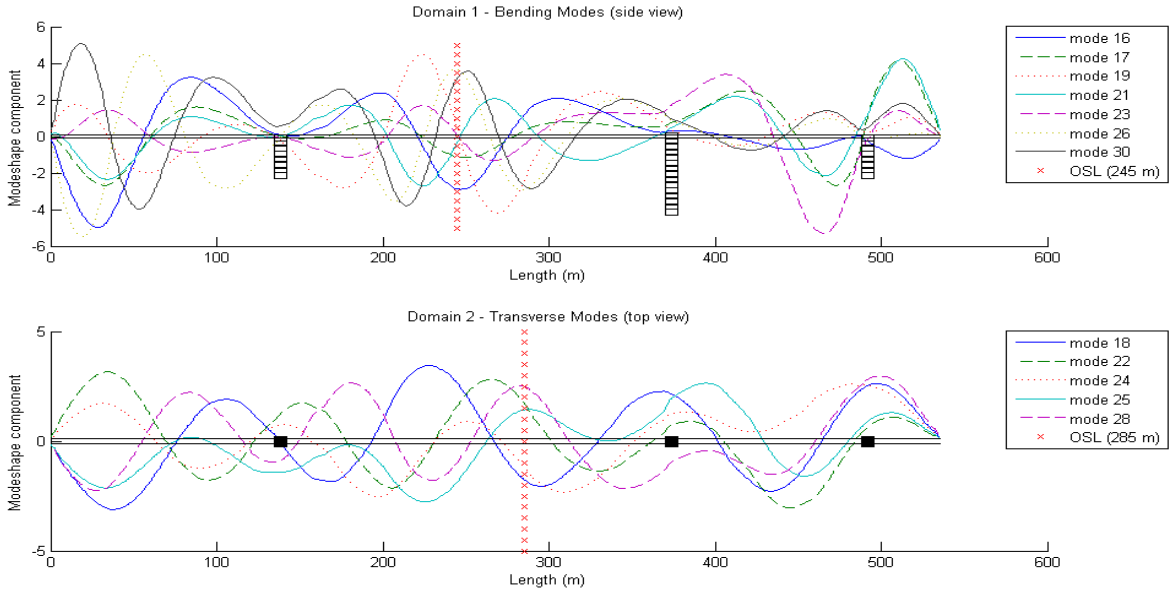

Figure 6.8: Optimal Sensor Locations for modes 16-30

In figures 6.7 and 6.8 we see the results for the optimal sensor locations for modes 1-15 and 16-30 respectively. The red vertical lines indicate the positions of the optimal locations. The search domain was confined at the middle of the bridge between 55m and 480m form the left end. Based on the results, the optimal sensor locations for two vertical sensors are at locations 225m and 245m. The sensor at 225m is optimal for identifying the bending modes that are contained within the lowest 15 modes, while the sensor location 245m is optimal for identifying the bending modes that are contained between the 16th and 30th modes. The two bending sensors are placed at the opposite sides of the bridge so that reference sensors for the torsional mode shapes are also available. The optimal sensor locations for two transverse sensors are at locations 255m (domain 2) and 285m. The sensor at 255m is optimal for identifying the transverse modes that are contained within the lowest 15 modes, while the sensor location at 285m is optimal for identifying the transverse modes that are contained between the 16th and 30th modes. It should be noted that a transverse sensor located at 305m is also near optimal for identifying the transverse modes contained between the 16th and 30th modes and at the same time improves the information contained in a couple of the lowest 15 modes that were missed by the optimal sensor location at 255m.

These positions are merely estimators of the best locations and will provide us with significant information content for identifying the corresponding modes accurately. We should remind that these positions pertain to the *reference* sensors. We can see that the results are quite intuitive; the vertical red lines cross the mode shapes in the points of most simultaneous activity, thus verifying the validity of the method.

Chapter 7

Conclusions

In this thesis, an attempt was made to gather all the major subjects regarding vibration measurement of structures and elaborate on them. Specifically, we started with a description of the measurement equipment and addressed several issues regarding its capabilities. Chapter 2 could be used as a guide to learn this specific measurement system by SYSCOM.

Next, we presented the theoretical model of the structure under consideration. This turns out to be a very important step of the vibration measurement process, mainly because the mode shapes predicted by the FEM model contribute to the Optimal Sensor Location methodology described in Chapter 6. Next, a brief summary of the theory of Operational Modal Analysis was presented, which is the theory that enables us to extract the modal properties of the structure from measured acceleration time histories. The auto and cross power spectral density functions are the primary data for model parameter identification based on output-only (ambient) vibration measurements. The modal identification methodologies used by the MITooL software are based on the minimization of an error function using a least squares minimization approach.

Chapter 5 deals with the problem of combining identified mode shapes from several different positions of the structure into the global mode shape vector. This is a common problem when dealing with large structures since we need to cover many more points than our available sensors. An efficient methodology is presented that results in a simple and easy to use equation for finding the optimal global mode shape vector from identified mode shape components from different parts of the structure.

Finally, in the last chapter it became apparent how the number and locations of the sensors can affect the quality of the measured time histories and consequently the results of modal analysis. An empirical method was first presented. Then an Information Theory approach was used to quantify the quality of various sensor configurations according to their Information Entropy. The best sensor configuration is chosen as the one which has the minimum Information Entropy.

Bibliography

[1] Au S.K. (2011), Assembling mode shapes by least squares, Mechanical Systems and Signal Processing 25 163–179.

[2] Beck J.L., May B.S., Polidori D.C. (1994), Determination of modal parameters from ambient vibration data for structural health monitoring, Proceedings of the 1st World Conference on Structural Control, Los Angeles, USA, 1395-1402.

[3] Beck J.L., Katafygiotis L.S. (1998), Updating models and their uncertainties—I: Bayesian statistical framework, Journal of Engineering Mechanics (ASCE) 124 (4) 455–461.

[4] Bleistein N., Handelsman R. (1986), Asymptotic Expansions for Integrals, Dover Publications, New York.

[5] Brincker R., Zhang L., Andersen P. (2001), Modal identification of output-only systems using frequency domain decomposition, Smart Materials and Structures 10 441-445.

[6] Ewins D.J. (2000), Modal Testing : theory, practice and application, Second Edition, Research Studies Press LTD.

[7] Hermans L., Van der Auweraer H., Guillaume P. (1998), A frequency-domain maximum likelihood approach for the extraction of modal parameters from output-only data, Proceedings of the 23rd International Seminar on Modal Analysis (ISMA23), 367-376

[8] Katafygiotis L.S., Yuen K.V. (2001), Bayesian spectral density approach for modal updating using ambient data, Earthquake Engineering and Structural Dynamics 30 (8) 1103-1123.

[9] Katafygiotis L.S., Papadimitriou C., Lam H.F. (1998), A probabilistic approach to structural model updating, International Journal of Soil Dynamics and Earthquake Engineering 17 (7–8) 495–507.

[10] Kelantonis V. (2010), Design and dynamic analysis of the Metsovo bridge using Finite Elements, Master Thesis, Department of Mechanical Engineering, University of Thessaly, Greece.

[11] Ljung L. (1999), System Identification: Theory for the User, Prentice-Hall, New York, USA.

[12] Lutes L., Sarkani S. (2004), Random Vibrations : Analysis of Structural and Mechanical Systems, Elsevier, Butterworth–Heinemann.

[13] Ntotsios E. (2009), Experimental modal analysis using ambient and earthquake vibrations: Theory, Software, and Applications, Master Thesis, Department of Mechanical Engineering, University of Thessaly, Greece.

[14] Papadimitriou C., Lombaert G. (2011), The effect of prediction error correlation on optimal sensor placement in structural dynamics, Mechanical Systems and Signal Processing.

[15] Papadimitriou C. (2004), Optimal sensor placement methodology for parametric identification of structural systems, Journal of Sound and Vibration 278 (4) 923–947.

[16] Papadimitriou C. (2005), Pareto optimal sensor locations for structural identification, Computer Methods in Applied Mechanics and Engineering 194 (12– 16) 1655–1673.

[17] Papadimitriou C., Beck J.L., Au S.K. (2000), Entropy-based optimal sensor location for structural model updating, Journal of Vibration and Control 6 (5) 781–800.

[18] Peeters B., Van der Auweraer H. (2005), Recent developments in operational modal analysis, EURODYN 2005, C. Soize and G.I Schueller (eds), Millpress, Rotterdam, 149-154.

[19] Qureshi Z.H., Ng T.S., Goodwin G.C. (1980), Optimum experimental design for identification of distributed parameter systems, International Journal of Control 31 21–29.

[20] Udwadia F.E. (1994), Methodology for optimal sensor locations for parameter identification in dynamic systems, Journal of Engineering Mechanics (ASCE) 120 (2) 368–390.